Calhoun
Institutional Archive of the Naval Postgraduate School

Calhoun: The NPS Institutional Archive

DSpace Repository

Theses and Dissertations | 1. Thesis and Dissertation Collection, all items

1966

Microwave backscatter from a capped dielectric lens

Ambrose, John Edward; Segelhorst, Herbert Edwin

Monterey, California. U.S. Naval Postgraduate School

http://hdl.handle.net/10945/9577

Downloaded from NPS Archive: Calhoun

http://www.nps.edu/library

Calhoun is the Naval Postgraduate School's public access digital repository for research materials and institutional publications created by the NPS community. Calhoun is named for Professor of Mathematics Guy K. Calhoun, NPS's first appointed -- and published -- scholarly author.

Dudley Knox Library / Naval Postgraduate School
411 Dyer Road / 1 University Circle
Monterey, California USA 93943

NPS ARCHIVE
1966
AMBROSE, J.

MICROWAVE BACKSCATTER FROM A CAPPED DIELECTRIC LENS

JOHN EDWARD AMBROSE
AND
HERBERT EDWIN SEGELHORD

LIBRARY
NAVAL POSTGRADUATE SCHOOL
MONTEREY, CALIF. 93940

DUDLEY KNOX LIBRARY
NAVAL POSTGRADUATE SCHOOL
MONTEREY, CA 93943-5101

This document has been approved for public release and sale; its distribution is unlimited.

MICROWAVE BACKSCATTER

FROM A CAPPED DIELECTRIC LENS

by

John Edward Ambrose
Commander, United States Navy
B.S., University of Maryland, 1951

and

Herbert Edwin Segelhorst
Lieutenant Commander, United States Navy
B.S., University of Missouri, 1957

Submitted in partial fulfillment
for the degree of

MASTER OF SCIENCE IN COMMUNICATIONS ENGINEERING

from the

UNITED STATES NAVAL POSTGRADUATE SCHOOL
May 1966

NPS ARCHIVE
1966
AMBROSE, J.

ABSTRACT

A specific application of a spherical dielectric lens provides the impetus for the development of a simple analytical method of predicting microwave backscatter from such a lens. The principles of geometric optics and stationary phase are presented as detailed in current literature. Geometric optics or ray tracing is then utilized in developing a unique method of determining the backscattered E field by the use of a computer program constructed for the CDC 1604 computer. Several models are constructed and tested in an anechoic chamber and on an outdoor radar backscatter range. The results of these tests are then compared to those of the computer program. The correlation of the predicted and measured E fields indicates the computer program to be a useful tool in the construction of a dielectric lens.

Library
U. S. Naval Postgraduate School
Monterey, California

DUDLEY KNOX LIBRARY
NAVAL POSTGRADUATE SCHOOL
MONTEREY, CA 93943-5101

TABLE OF CONTENTS

Section		Page
1.	Introduction	7
2.	Optical Paths	11
3.	Development of the Sulphur Lens	28
4.	Spherical Lens of Varied Dielectric Constant	31
5.	Compound Spherical Lens of Varied Dielectric Constant	38
6.	Results and Conclusions	63
7.	Bibliography	79
	Appendix I	80
	Appendix II	91
	Initial Distribution List	94
	Form DD 1473	95

LIST OF ILLUSTRATIONS

Figure		Page
1.1	Bistatic Angle	8
2.1	Emergent Rays from a Sphere	12
2.2	Apparent Radii of Curvature of Refracted Rays	14
2.3	Plane Wave Incident Upon an Irregular Surface	17
2.4	Apparent Radii of Curvature within a Dielectric Sphere	18
2.5	Axial Rays	21
2.6	Glory Ray	22
2.7	Toroidal Wave Front of the Glory Ray	24
3.1	Missile Nose Section	28
4.1	Backscatter Versus Electrical Size	31
4.2	Stationary Ray	33
4.3	Emergent Angle Versus Incident Angle	34
4.4	Emergent Angle Versus Dielectric Constant for a Spherical Lens	36
5.1	Maximum Aspect Angles	40
5.2	Internal Ray Paths	42
5.3	Projection of Lens Face onto x, y Plane	46
5.4	Vector Components of Incident Radiation (face on view)	48
5.5	Co-ord System for Summing Far Field Contribution of each Emerging and Reflected Ray	54

Figure		Page
5.6	Ray Paths	59
6.1	Measured Radar Return for a Napthalene Sphere	67
6.2	Measured Radar Return for a Nylon Sphere	68
6.3	Measured Radar Return for a Polystyrene Sphere	69
6.4	Measured Radar Return for a Lucite Spheroid ($R_2 = 3.83"$)	70
6.5	Measured Radar Return for a Lucite Spheroid ($R_2 = 3.7"$)	71
6.6	Monostatic Radar Return	72
6.7	Radar Cross Section Versus Bistatic Angle for a Napthalene Sphere	73
6.8	Radar Cross Section Versus Bistatic Angle for a Nylon Sphere	74
6.9	Radar Cross Section Versus Bistatic Angle for a Polystyrene Sphere	75
6.10	Radar Cross Section Versus Bistatic Angle for a Lucite Spheroid ($R_2 = 3.83"$)	76
6.11	Radar Cross Section Versus Bistatic Angle for a Lucite Spheroid ($R_2 = 3.7"$)	77
6.12	Comparison of Computed and Measured Monostatic Return	78
I.1	Stationary Phase Front	81
I.2	Phasor Addition	81
I.3	Rear Axial Ray	86
I.4	Stationary Ray	87

1. Introduction

Numerous studies of microwave backscatter by dielectric bodies have been prompted by the necessity to understand normal radar phenomena; i.e., backscatter from ice crystals, composite bodies, and plasma enclosed bodies. These studies deal almost entirely with the monostatic return from such masses. The need for, and understanding of, bistatic characteristics are apparent as soon as there exists a spatial separation between the transmitter and receiver. This separation comes about in several applications of passive backscatter augmentation systems, such as communications relay and as an enhanced target for radar controlled missiles. This project was initiated to develop a simple, analytical tool yielding approximate results which would be useful in the design of dielectric lenses. The method of analysis presented is applicable to a general class of dielectric lens which meet the following criteria:

(a). Physical dimensions large in terms of wave length.

(b). Material of constant index of refraction for a given frequency.

(c). Shape readily expressible in mathematical form.

The specific analysis presented is based on the requirements of a particular passive radar augmentation system.

A radar directed attack on a drone-type target requires the drone to present a realistic and effective simulation of the ultimate enemy target. Although high speed drones of such size could be constructed,

the excessive cost would preclude destruction necessary for effective attack simulation. Use of active augmentation systems has failed due to excessive cost, difficult installation and maintenance, and doubt of failure source in aborted or unsuccessful attacks. These failures prompted a search for a suitable passive augmentation system. Accordingly, the Naval Missile Test Center, Point Mugu, California, issued a design requirement which contained the following pertinent characteristics:

Passive Augmenter

Size - 7 inches in maximum dimension

Return when illuminated with 10 GHz radar

Monostatic - 2 to 5 square meters

Bistatic - Minimum of .5 square meters at 10° bistatic angle, vertically polarized

Aperture - 120° forward angle

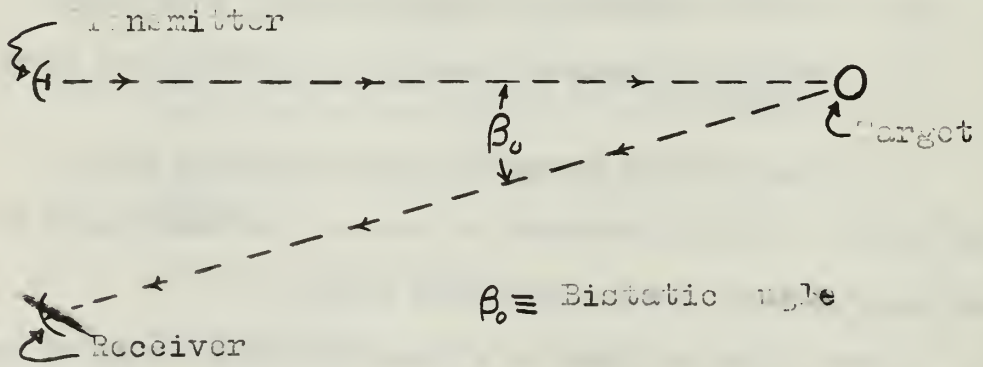

Figure 1.1

Bistatic angle

Two distinct systems were designed and tested under this request; a spherical plastic lens of uniform dielectric constant, and a spheroid formed of compressed sulphur. The choice of these materials was dictated by several features to be explained within this report. The spheroidal sulphur lens was selected on the basis of superior performance. The need for additional improvement of bistatic cross section of this lens led to the discovery that the design was primarily empirical, and additional "cut and try" testing of doubtful value.

Classical boundary solutions have been presented for dielectric lens of simple shapes, such as the sphere and cylinder. These solutions become tedious and involved for shapes large in terms of wave length. Such solutions have not been generally extended to materials of dielectric constant $\epsilon_r > 2$. The method of analysis generally used is that of modified geometric optics, wherein principles of physical optics are employed where geometric optics do not suffice. [8]. These studies are concerned with the radar cross section of the lens and are, therefore, usually limited to monostatic characteristics.

Inasmuch as an understanding of the lens action of a dielectric body is required, the modified geometric optics theory of Thomas [9] and Atlas [2] et al, is first presented for the monostatic case in the dielectric sphere. Adaptations of this theory are then applied in the initial experimental efforts to obtain better bistatic return.

Predicted performance of a lens is then obtained in terms of radii of front and back surfaces and dielectric constant, and developed in a program prepared for the CDC 1604 computer. Full scale models were constructed of polystyrene, nylon, napthalene, and lucite and tested on the backscatter range at Micronetics Inc., San Diego, California, and in an anechoic chamber at Naval Missile Test Center, Point Mugu, California.

2. Optical Paths

Analysis of electromagnetic waves by geometrical optics relies on Fermat's principle which states that the optical ray or rays from a source at a point P_1 to a point of observation P_2 is the curve along which the optical path length is stationary with respect to infinitesimal variations in path. Optical path length along curve Γ between points P_1 and P_2 is described as $\Delta L = \int_\Gamma \eta \, |ds|$ where η is the refractive index. In the case of isotropic homogeneous media, with which we will deal exclusively, η is constant and the rays are straight lines.

Geometric analysis utilizes this principle and Snell's Law, which may be stated by $\eta_0 \sin \theta_0 = \eta_1 \sin \theta_1$ where η_0 and η_1 are the respective refractive indices of the two mediums. θ_0 is the angle of incidence and θ_1 the angle of refraction. Ray tracing by the use of Fermat's principle and Snell's Law involves considering each ray with its angles of incidence, reflection, and refraction as it traverses the medium. The number of rays considered are, in the interests of simplicity, usually small in the studies available. In fact, for those dielectric constants for which the only backscatter ray is colinear with the incident ray, it is the only ray considered. There are two of these specular rays for a sphere, one from the front surface and one from the back surface. This approach becomes invalid and physical optics must be introduced, as the dielectric constant is increased and a glory ray becomes

evident. The glory ray appears as a doughnut or toroidally shaped wave front formed as indicated in Figure 2.1. It exists for refractive indices between $(2)^{1/2}$ and 2 since, by Snell's Law

(2.1) $\eta_1 \sin\theta_1 = \eta_2 \sin\theta_2 \qquad \theta_1 = \frac{\theta_0}{2}$

$$\cos\theta_1 = \cos\frac{\theta_0}{2} = \frac{\eta_1}{2}$$

(2.2) $$\cos\theta_1 = \frac{\eta_1^2 - 2}{2} \qquad \therefore \sqrt{2} \leq \eta_1 \leq 2$$

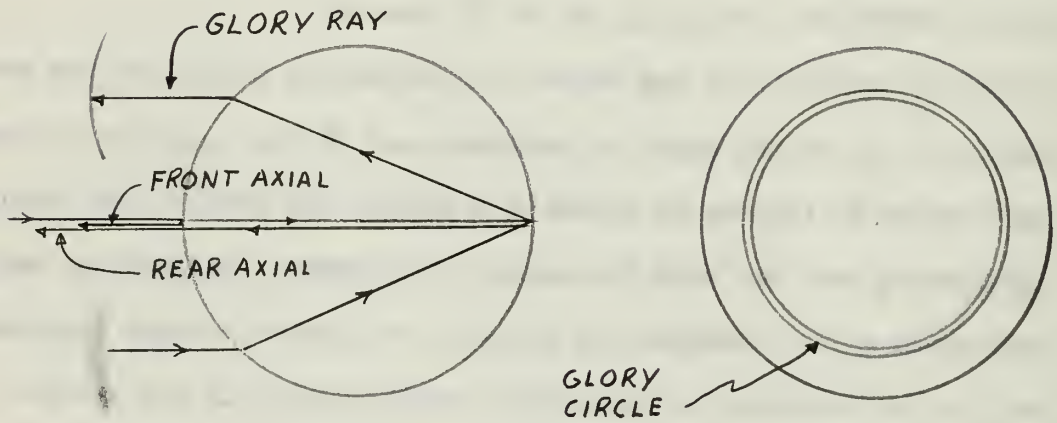

Figure 2.1

Emergent rays from a sphere

The electromagnetic wave is considered as an equiphase surface propagating into a succeeding equiphase surface. The incident ray, reflected ray, refracted ray, and the normal to the plane of incidence are all in the same plane, the plane of incidence. Fields are calculated for the reflected rays and the internally refracted emergent rays. The amplitude of the rays, relative to some incident amplitude, is computed by applying the laws of conservation of energy along a ray tube. The phase is determined, relative to a selected reference point, by use of the propagation constant ($k = 2\pi/\lambda$) and the distance plus the phase shift within the lens. The radar cross section σ of a sphere is defined as $\sigma = \lim_{\ell \to \infty} 4\pi \ell^2 \frac{|E^s|^2}{|E^i|^2}$ and, expressed as the vector sum of the backscattered rays related to cross sectional area, is:

(2.3)
$$\frac{\sigma}{\pi a^2} = \left[\underset{\substack{\text{front} \\ \text{axial}}}{\sigma^{1/2}} + \underset{\substack{\text{rear} \\ \text{axial}}}{\sigma^{1/2} e^{j\phi_1}} + \underset{\text{glory}}{\sigma^{1/2} e^{j\phi_2}} + \underset{\text{stationary}}{\sigma^{1/2} e^{j\phi_3}} \right]^2$$

The field of an individual ray in the far zone may be expressed in the form

(2.4) $$U(\ell) = \tau A_0 e^{j\phi_0} F(\ell) e^{-jk\ell}$$ where

A_0 is the reference amplitude

τ is the total transmission coefficient

ϕ_0 is the reference phase

$F(\ell)$ is the spatial attenuation factor

e^{-jkl} is the spatial phase delay factor

$e^{j\omega t}$ time dependence is assumed

The spatial attenuation factor is dependent upon the nature of the reference equiphase surface. This surface will generally have two principal radii of curvative, ρ_1 and ρ_2, developing two convergent rays as shown in Figure 2.2-b using a completely forward transmitted ray for clarity.

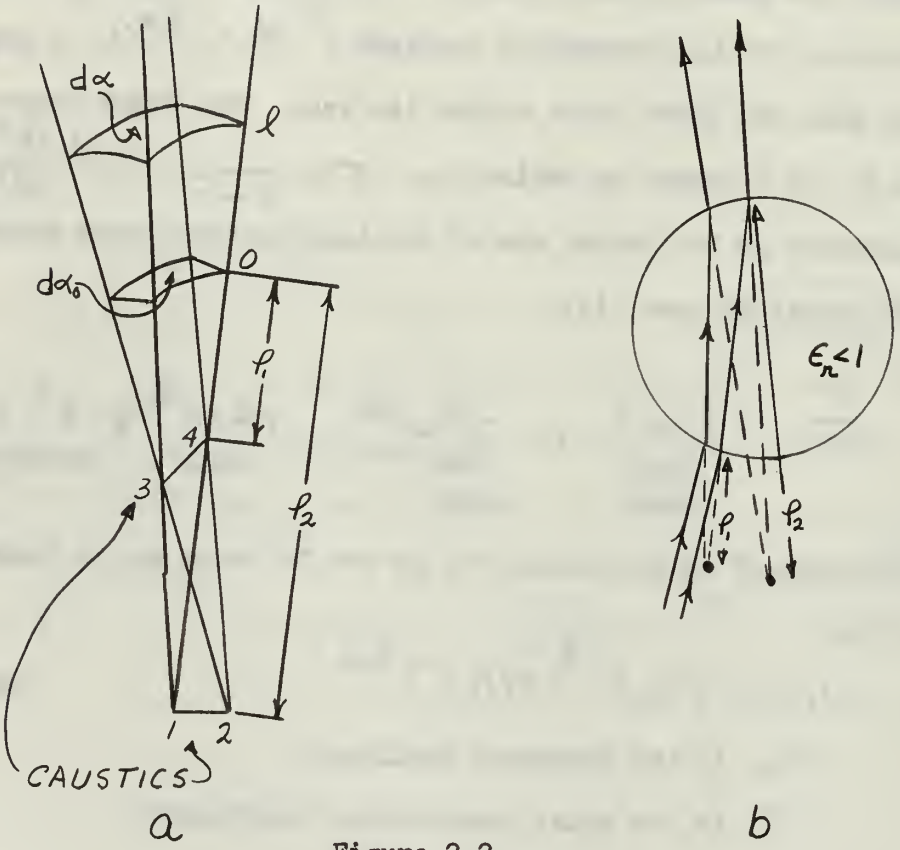

Figure 2.2

Apparent radii of curvature of refracted rays

The energy within a tube of rays as shown in Figure 2.2 must remain constant. The wave front will diverge in a cone-shaped dispersion, the parameters of which are dependent upon the hypothetical point sources ρ_1 and ρ_2, Figure 2.2. Consequently, if Ao is the field amplitude at the differential cross section $d\alpha_0$, and A the amplitude at $d\alpha$, then $A_0^2\, d\alpha_0 = A^2 d\alpha = \text{constant}$. For small $d\alpha_0$ and $d\alpha$

$$\frac{d\alpha}{d\alpha_0} = \frac{(\rho_1+\ell)(\rho_2+\ell)}{\rho_1 \rho_2}$$

(2.5) $$F(\ell) = \frac{A}{A_0} = \left[\frac{\rho_1 \rho_2}{(\rho_1+\ell)(\rho_2+\ell)}\right]^{1/2}$$

(2.6) $$U(\ell) = \tau A_0 e^{j\phi_0} \left[\frac{\rho_1 \rho_2}{(\rho_1+\ell)(\rho_2+\ell)}\right]^{1/2} e^{-jk\ell}$$

The caustics or crossings of the rays require the introduction of $-\pi/2$ phase shift where $\ell = -\rho_1$ or $\ell = -\rho_2$ in order for geometric optics to apply. The fields then become

(2.7) $$U(\ell) = \tau A_0 e^{j\phi_0} \left[\frac{\rho_1 \rho_2}{(\rho_1+\ell)(\rho_2+\ell)}\right]^{1/2} e^{-j\pi/2}\, e^{-jk\ell}$$

The amplitude of the backscattered rays may be determined in terms of the total transmission of the ray; consisting of τ_{12} through

the front surface, R_{21} reflection at the rear surface, $\tilde{\tau}_{21}$ emerging from the front surface, and a total spatial attenuation factor $F(\ell)$ due to the change in the wave front's principal radii of curvature.

The resultant phase is determined by introducing $-\pi/2$ phase shift for each caustic encountered in addition to the shift due to normal delay factors relative to the phase at a selected reference point.

Transmission coefficients are determined as Fresnel reflection coefficients for parallel and perpendicular polarization. [9].

(2.8) $$R_{01}^{\parallel}(\theta_0) = \frac{\epsilon_r \cos\theta_0 - \sqrt{\epsilon_r - \sin^2\theta_0}}{\epsilon_r \cos\theta_0 + \sqrt{\epsilon_r - \sin^2\theta_0}}$$

(2.9) $$R_{01}^{\perp}(\theta_0) = \frac{\cos\theta_0 - \sqrt{\epsilon_r - \sin^2\theta_0}}{\cos\theta_0 + \sqrt{\epsilon_r - \sin^2\theta_0}}$$

(2.10) $$\tilde{\tau}_{01}^{\parallel} = 1 + R_{01}^{\parallel}(\theta_0)$$

(2.11) $$\tau_{01}^{\perp} = 1 + R_{01}^{\perp}(\theta_0)$$

Incidence of a field U^i on point Q of a dielectric surface may be taken as an example. See Figure 2.3. The amplitude and phase

$A_1 e^{j\phi_1}$ of the reflected ray is given by

(2.12) $$A_1 e^{j\phi_1} = R_{12}(\theta_0)\, \sqcup^i Q$$

and the refracted ray by

(2.13) $$A_1' e^{j\phi_1'} = T_{12}(\theta_0)\, \sqcup^i Q \sqrt{\frac{\cos\theta_0}{\cos\theta_1}}$$

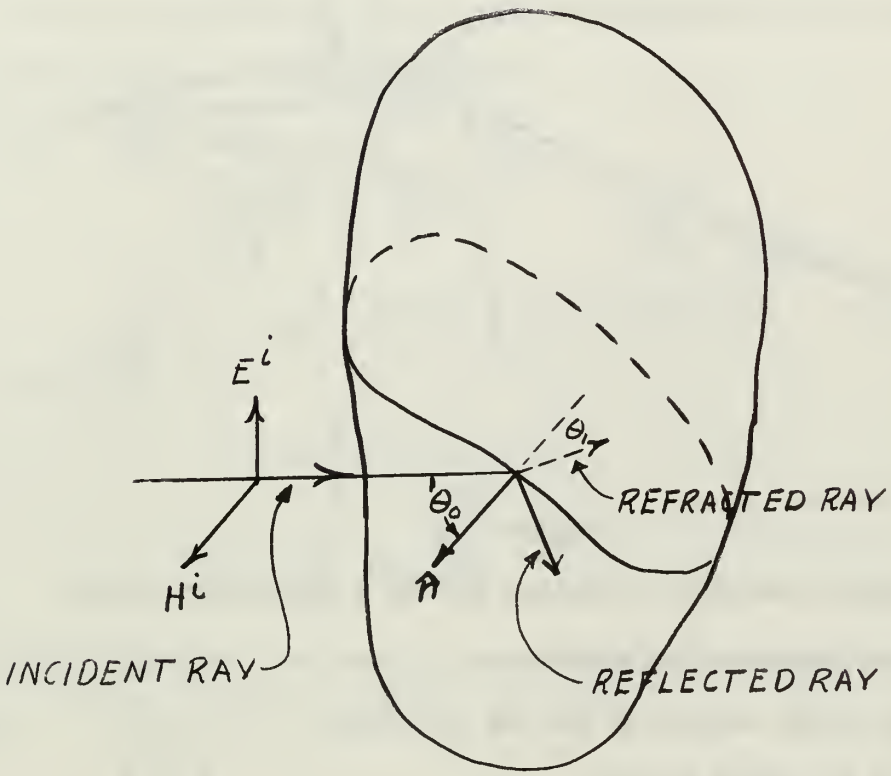

Figure 2.3

Plane wave incident upon an irregular surface

The new radii of curvature ρ_1 and ρ_2 required to evaluate $F(\ell)$ are found from the geometry of the interface. The two dimensional case for the sphere, or cylinder, is illustrated in Figure 2.4.

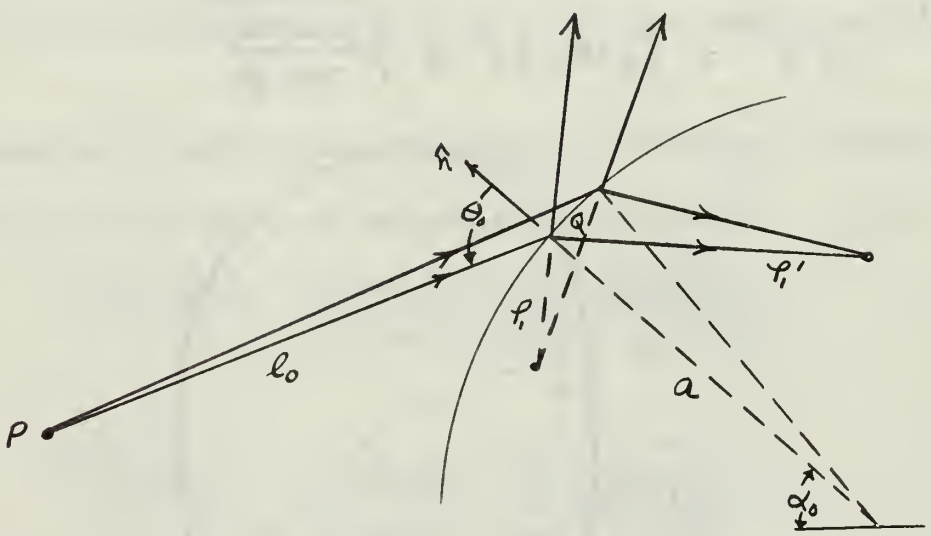

Figure 2.4

Apparent radii of curvature within a dielectric sphere

a = radius of the sphere

α_0 = angle between $\hat{N}$ and the horizontal

P is the field source

Q is the point of incidence

$$\frac{\Delta(\theta_0-\alpha)\,\ell_0}{\cos\theta_0} = \frac{\Delta(\theta_0+\alpha)\,\rho_1}{\cos\theta_0} = a\,\Delta\alpha$$

(2.14) $$\frac{1}{\rho_1} = \frac{2}{a \cos\theta_0} + \frac{1}{l_0}$$

$$\frac{\Delta(\theta_0 - \alpha) l_0}{\cos\theta_0} = \frac{\Delta(\alpha - \theta_1)\rho'}{\cos\theta_1} = \text{a} \Delta\alpha$$

(2.15) $$\frac{1}{\rho_1'} = \frac{1 - d\theta_1/d\theta_0}{a \cos\theta_1} - \frac{\cos\theta_0 \; d\theta_1/d\theta_0}{l_0 \cos\theta_1}$$

It is now possible to find the field parameters for the front axial and rear axial rays. Figure 2.5.

(a). Front axial ray

$$A_1 F(l)_1 e^{j\Phi_1} e^{-jkl}$$

$$A_1 = A_0[-R_1''(0^\circ)] = A_0[R^{\perp}(0^\circ)]$$

$$= A_0\left[\frac{1-n}{1+n}\right]$$

$$\rho_1 = \frac{a}{2}\cos\theta_0$$

As the wave diverges, the energy density decreases in proportion to

(2.16) $$\left[\frac{\rho_1}{l}\right]^{1/2}$$

due to spreading in the plane of Figure 2.4 and in proportion to the square root of the cone periphery which equals

(2.17) $$\left[\frac{2\pi a \sin\theta_0}{2\pi l \sin\beta}\right]^{1/2} = \left[\frac{a \sin\theta_0}{l \sin\beta}\right]^{1/2}; \quad \beta = (\pi - 2\theta_0)$$

$$F(\ell) = \left[\frac{\ell_1}{\ell}\right]^{1/2}\left[\frac{a \sin\theta_0}{\ell \sin\beta}\right]^{1/2} = \frac{a}{2\ell}$$

(2.18) $$B = \left(\frac{a}{2\ell}\right)\left(\frac{2\ell}{a}\right) = 1 \qquad B \equiv \frac{2\ell}{a} F(\ell)$$

$$\phi_1 = 2ka\cos\theta_0 = 2ka$$ (referred to center of sphere)

(2.19) $$U(\ell_1) = A_0\left(\frac{1-\eta}{1+\eta}\right) e^{-j2ka} e^{-jk\ell}$$

(2.20) $$U(\ell_1) = A_1 B_1 e^{\phi_1'}$$

(b). Rear axial ray

The rear axial ray is expressed as

$$U(\ell)_3 = A_3 F(\ell)_3 e^{j\phi_3} e^{-jk\ell}$$

The multiple bounce rear axial ray

$$U(\ell)_5 \doteq 0.001\ U(\ell)_3$$

and is considered negligible.

$$A_3 = -R_1^{\perp}(0°)\left[1 - \left\{R_1^{\perp}(0°)\right\}^2\right] A_0 = \frac{4\eta(1-\eta)}{(1+\eta)^3} A_0$$

$$F(\ell)_3 = \left(\frac{a}{2\ell}\right)\frac{\eta}{2-\eta}$$ Derivation in Appendix I

$$B = \frac{\eta}{2-\eta}$$

$$\phi_3 = 2ka(1-2\eta) + \pi$$

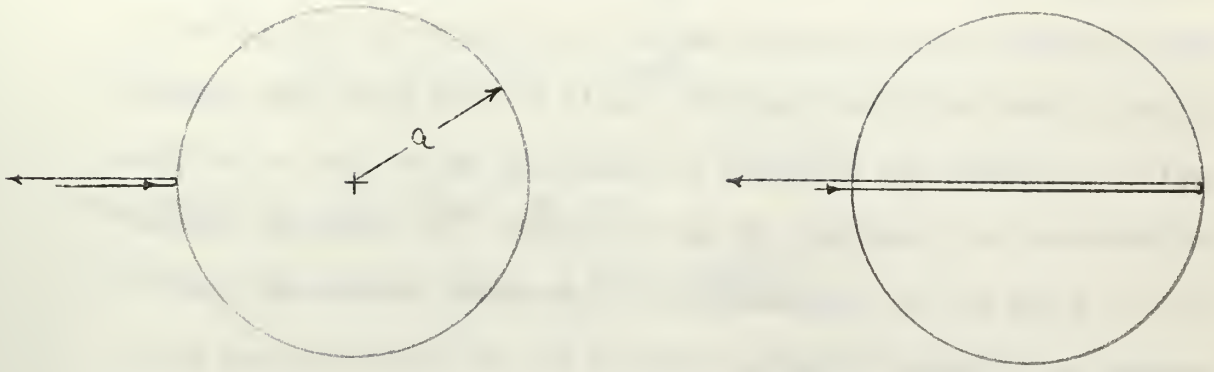

a
front axial ray

b
rear axial ray

Figure 2.5

Axial rays

The far field due to this ray proves to be larger than that obtained from an aperture distribution with uniform phase and is, therefore, incorrect. [2]. Consideration of the two-way attenuation, due to the absorption coefficient K, will introduce a factor of $e^{-4\alpha K}$ where $K = \frac{2\pi}{\lambda} a$

The field due to the rear axial ray is then

(2.21)
$$U(\ell)_3 = U^i e^{j\phi_3} \left(\frac{a}{2\ell}\right) \frac{4n^2(1-n)}{(1+n)^3(2-n)} e^{-(jk\ell + 4\alpha K)}$$
$$= A_3 B_3 e^{j\phi_3'}$$

The glory ray and stationary ray are products of a three di-

mensional body and appear as a ring source. Application of geometric optics results in one infinite radius of curvature leading to an infinite field which is incorrect. It is at this point that physical optics, utilizing the principle of stationary phase, must be utilized to determine the parameters of the far field. The equiphase surface for the glory ray is approximated by a quadratic expression which results in a Fresnel integral, and that for the stationary ray by a cubic expression which results in an Airy integral which is tabulated. [1]. These derivations are rather lengthy and are given in Appendix I. The glory ray and stationary ray are monostatic characteristics and are presented for an understanding of the overall lens action.

(c). Glory ray

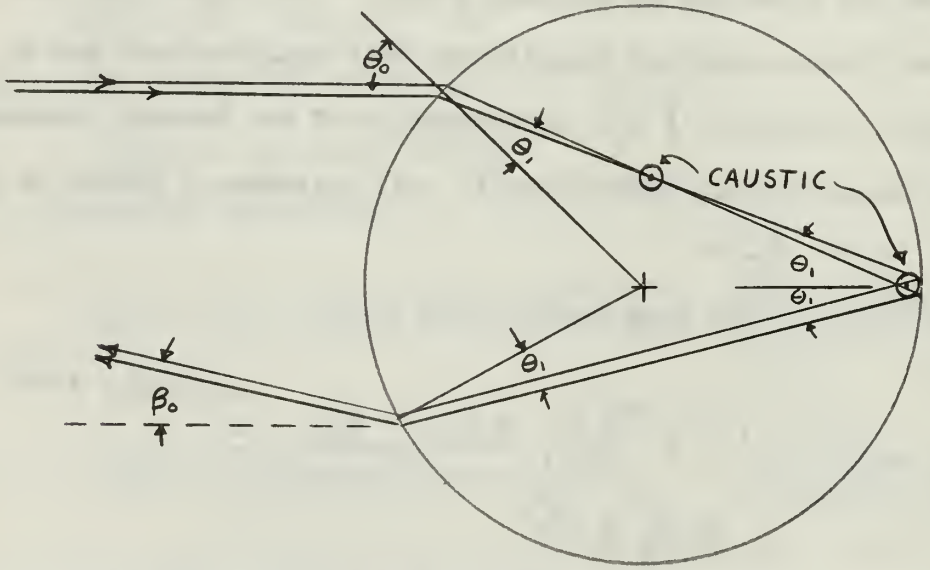

Figure 2.6

Glory ray

(2.22) $$\beta_0 = \pi + 2(\theta_0 - 2\theta_1)$$

(2.23) $$\gamma = \pi + \theta_0 - 4\theta_1$$

The glory ray occurs when $\beta_0 = 0$

(2.24) $$\beta_0 = 0 = \pi + 2(\theta_0 - 2\theta_1)$$

Snell's Law may now be used to find the incident angle of the glory ray. This ray occurs in the sphere with $\epsilon_r = 2.54$ at $\theta_0 = 72.8^\circ$

$$\theta_1 = 36.4^\circ$$

The single bounce ray must cross two caustics, Figure 2.6, requiring a phase shift of 180°. The total phase shift, referring to the surface as zero phase is

(2.25) $$\phi_1 = \frac{2\pi}{\lambda}(2a)\left(1 - \frac{3\sqrt{\epsilon_r}\cos\theta_0}{\cos\theta_1}\right)\cos\theta_0 + \pi + \frac{\pi}{4}$$

and for the double bounce ray which occurs for $\sqrt{\epsilon_r} < 1.33$

(2.26) $$\phi_1' = \frac{2\pi}{\lambda}(2a)\left(1 - \frac{4\sqrt{\epsilon_r}\cos\theta_0}{\cos\theta_1}\right)\cos\theta_0 + \frac{3}{2}\pi + \frac{\pi}{4}$$

The ray path shown in Figure 2.6 is in a single plane. As this cross section is rotated, the glory and stationary rays appear as

rings of equal phase. Geometric optics may not be used to sum the contribution of all these rays, but may be used to find the contribution of a single ray within the ring.

The shape of the toroidal wave front is determined by ρ_1, Figure 2.7.

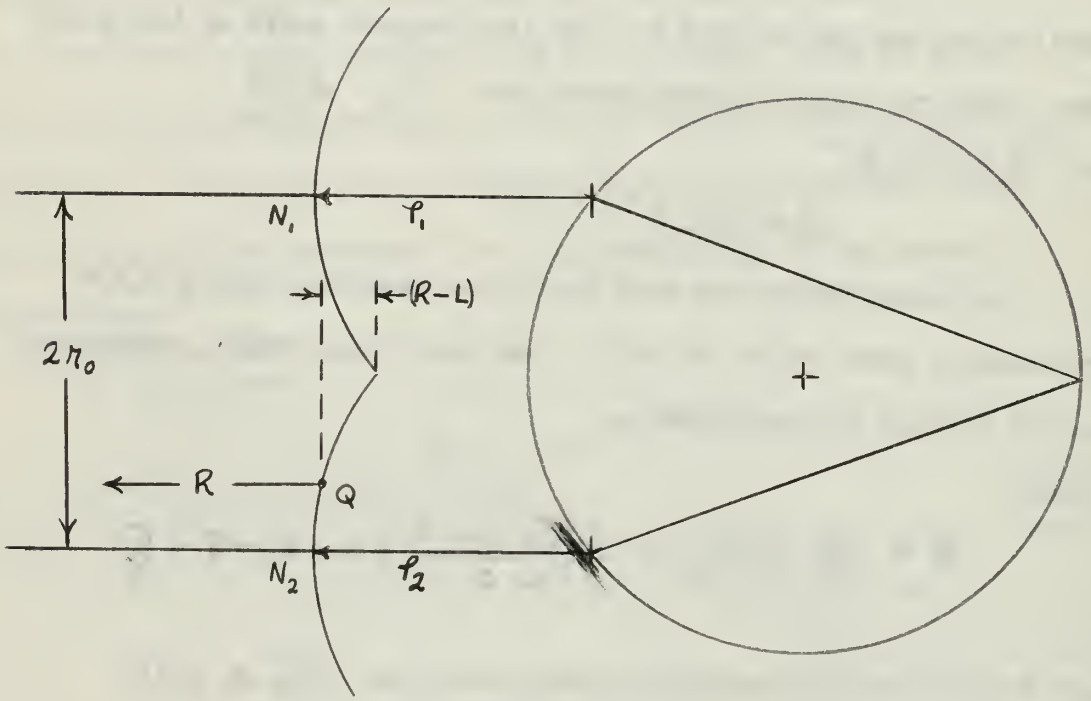

Figure 2.7

Toroidal wave front of the glory ray

The spatial attenuation factor may then be determined from

(2.27)
$$F(\ell)_n = \frac{1}{\lambda \ell}\left| \iint_{\delta_n} e^{-j k \psi}\, ds \right|$$
$$= \frac{1}{\lambda \ell}\, 2\pi \int_{r_0}^{r_0+\Delta r} r\, e^{-j\left[\frac{k (r-r_0)^2}{2\rho_1}\right]}\, dr$$
$$= \frac{2\pi r_0}{\lambda \ell} \int_{-\infty}^{\infty} e^{-j \frac{k (r-r_0)}{2\rho_1}}\, dr$$

(2.28)
$$F(\ell)_n = \frac{a\, 4\pi r_0}{2\ell\, a} \left[\frac{\rho_1}{\lambda}\right]^{1/2}$$

Derivation in Appendix I

(2.29)
$$B_n = \frac{4\pi r_0}{a} \left[\frac{\rho_1}{\lambda}\right]^{1/2}$$

A weighted average of the transmission coefficients with respect to ϕ must be used as the polarization changes as the cross section is rotated; that is, for a single internal reflection

(2.30)
$$R_{12}(\theta_1) = \frac{1}{2}\left[R_{12}^{\perp}(\theta_1) + R_{12}^{\parallel}(\theta_1)\right]$$

or for a combination of reflection and transmission

(2.31)
$$T_{12} R_{21} T_{21}\,(\theta_0) = \frac{1}{2}\left[T_{12}^{\perp} R_{12}^{\perp} T_{21}^{\perp} - T_{12}^{\parallel} R_{21}^{\parallel} T_{21}^{\parallel}\right]$$

therefore

(2.32) $$A_7 = A_0 T_{12} R_{21} T_{21}(\theta_0) \left[\frac{\Delta\theta_0}{\Delta\gamma}\right]^{-1/2}$$

and the field

(2.33) $$U(\ell)_7 = U^i T_{12} R_{21}(\theta_0) \frac{4\pi\pi_0}{2} \left[\frac{\rho_1}{\lambda}\right]^{1/2} e^{j\phi_7} e^{-jk\ell} e^{4\alpha K}$$

$$\left[1 - 4\frac{d\theta_1}{d\theta_0}\right]^{-1/2} = A_7 B_7 e^{j\phi_7}$$

(d). Stationary rays

The amplitudes for the far fields of the stationary rays are determined, as were those for the glory rays, by applying a resultant transmission and reflection coefficient. The relative phase also is determined, as was glory ray phase, by introducing a $\frac{\pi}{2}$ phase shift at each caustic and calculating normal shift within the two mediums. The amplitude is identical to that of the glory ray. The phase

(2.34)

$$\phi_9 = ka(1 - \cos\theta_0) + 3ka(2\cos\theta_1) + ka(1 - \cos\gamma) + \pi$$

$F(\ell)$ for the stationary or rainbow ray must be determined by use of Equation 2.27 and is derived in Appendix I as

(2.35) $$F(\ell)_9 = \frac{8\pi\gamma_0 S}{\lambda a} A_i(z)$$

(2.36) $$A_i(z) = \frac{1}{2}\int_{-\infty}^{\infty} e^{-j\left(zt - \frac{t^3}{3}\right)}\, dt$$

$$S = \left[\frac{a^{1/2}}{kh}\right]^{1/3} \qquad h = \frac{3\tan\theta}{4\cos^2\theta_0}$$

$$z = k\,\Delta\theta_S \qquad \theta_S \equiv \text{emergent angle}$$

(2.37) $$U(\ell)_q = U^i \tau_{12} R_{21} \tau_{21}(\theta_0)\left[1 - 4\frac{d\theta_1}{d\theta_0}\right]^{-1/2}\left[\frac{8\pi r_0 S}{\lambda a}\right.$$

$$\left. A_i(z)\, e^{j\phi_q}\, e^{-jk\ell}\, e^{-4\alpha K}\right] = A_q B_q e^{j\phi'_q}$$

The echo area of the sphere which is defined as

$$\sigma = \lim_{\ell\to\infty} 4\pi\ell^2 \frac{|E^A|^2}{|E^0|^2}$$

may be expressed as

(2.38)

$$\frac{\sigma}{\pi a^2} = \left| A_1 B_1 e^{j\phi'_1} + A_3 B_3 e^{j\phi'_3} + A_7 B_7 e^{j\phi'_7} + A_9 B_9 e^{j\phi'_9} \right|$$

It is obvious that the glory ray is not the primary contributor for the bistatic return as it is for the monostatic return. The principle effort of this study, as detailed in later sections of the report, is directed toward analyzing the bistatic return within the region of zero to 20° bistatic angle.

3. Development of the sulphur lens

Geometric optics and ray tracing were used by Micronetics in developing the original lens. The maximum diameter was determined by the missile diameter. See Figure 3.1.

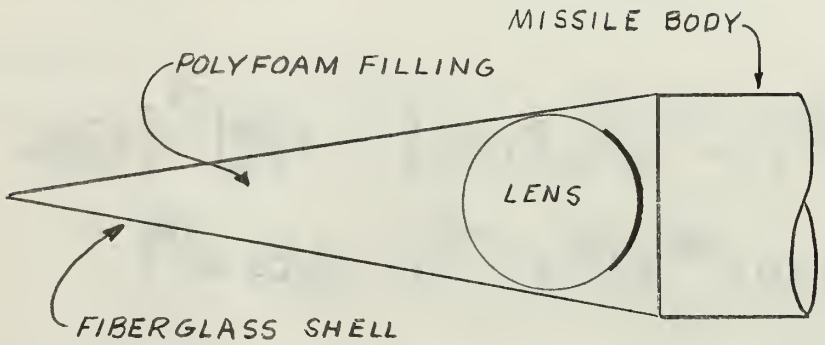

Figure 3.1

Missile nose section

The material for construction was selected for dielectric constant and low loss tangent. The desired dielectric constant was approximated as being $2 < \epsilon_r < 4$ and the loss tangent as low as possible. Sulphur was chosen with a dielectric constant of 3.8 and a loss tangent of 2×10^{-5} at a frequency of ten gigacycles. This dielectric constant, listed by Von Hipple, [10] is for solid sulphur. The material ultimately used was powdered or flowers of common sulphur. The lens was manufactured by compressing the sulphur in a mold. The average dielectric constant of the lens is a function of the molding

pressure. The dielectric constant at a point within the lens is an unknown function of position. The dielectric constant of chip cut from a sulphur lens was measured by the authors and found to be 2.36. No attempt was made to determine dielectric constant as a function of position.

The design was not predicated on measured dielectric constant, the density being varied to produce maximum response. The lens was formed and tested on a backscatter range where monostatic and five degree and ten degree bistatic characteristics were measured. The monostatic response of the spherical lens was very good, giving a return of approximately eight square meters, but the bistatic response fell below the minimum required cross section of .5 square meters. Reasoning that the monostatic response would be decreased and the bistatic response possibly increased by deformation or detuning the spherical lens, Micronetics next introduced a cylindrical section one half inch in thickness into the center of the sphere. This reduced the monostatic return from eight to six square meters and increased the bistatic response to 4 m^2 at five degree bistatic angle, 2m^2 at $7\frac{1}{2}^o$ and 1m^2 at ten degrees. Inasmuch as this performance fulfilled the specification and proved superior to all other models submitted, this shape was placed in production. The flowers of sulphur are purchased in batch lots after testing a model constructed from a sample thereof. The required density, and thereby dielectric

constant, is obtained by compressing a given weight of powder into the same mold for each lens. The lens is then trimmed, rear cap fitted and encased in polyfoam within the nose cone.

The difficulty of maintaining uniformity in the batch lots of sulphur and adequate tolerance in the lens manufacture led to a search for a plastic material with the desired characteristics. The need for symmetry of performance for all forward attack angles limited this study to spherical lens forms. The selection of spherical forms led to a natural division of this project into two parts. The first is a consideration of true spheres of various materials to study the effect of different dielectric constants on bistatic return. The second part is a study of compound biradial spherical shapes of various radii.

4. Spherical lens of varied dielectric constant

The first method is consistent with the explanation of the backscatter contributions explained in Section 2, and utilizes the system of notation of the references cited. The rear axial, front axial and glory rays are considered the principal contributors for the monostatic return. These rays require only the selection of a dielectric constant, ϵ_r, such that $2 < \epsilon_r < 4$ (from Equation 2.2). The maximum allowable diameter of the lens was seven inches. The monostatic return of a spherical dielectric lens with $2 < \epsilon_r < 4$ is shown in Figure 4.1 as demonstrated by Atlas. [3].

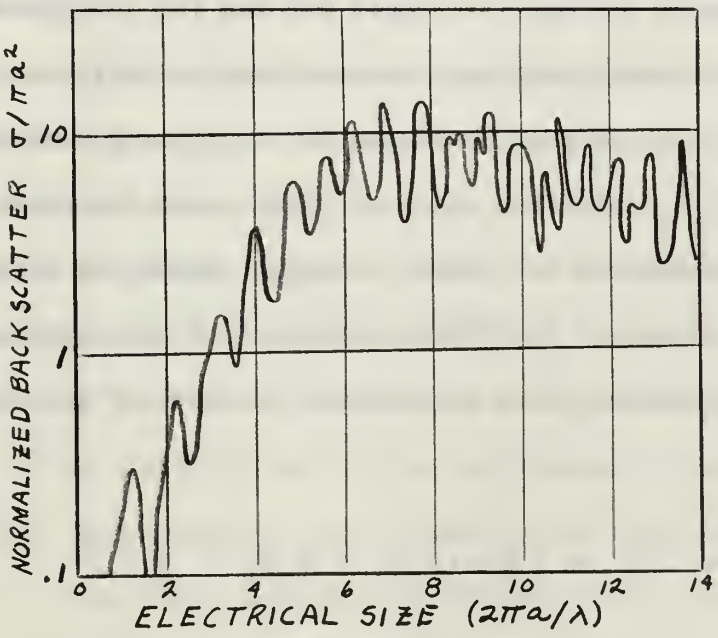

Figure 4.1

Backscatter versus electric size

The overall return is a function of the cross sectional area. The maximum area and, therefore, the maximum diameter of seven inches, was chosen.

Variable parameters remaining were dielectric constant, movable rear cap, front interference or tuning strips, and internal voids. The movable rear cap was not considered due to the difficulty in maintaining the required spacing and empirical tuning requirements. The front tuning strips were rejected as reducing the overall performance, and the internal voids as lacking symmetrical performance over the face of the lens as well as difficulty of manufacture. Variation of dielectric constant was selected for investigation. The contributors to bistatic performance are the stationary ray and the individually refracted rays. The stationary ray, representing an equiphase surface or ring source on the face of the lens, is the primary contributor.

Selection of a dielectric constant which would concentrate the stationary ray within the ten degree bistatic region was first suggested by Chief Scientist Mr. William Bradford of Micronetics, Inc.

The emergent angle, β of Figure 4.2, for the off axis ray may be expressed as

(4.1) $$\beta = \pm[-2(q+1)\theta_1 + 2\theta_0 + q\pi]$$

where q is the number of internal bounces.

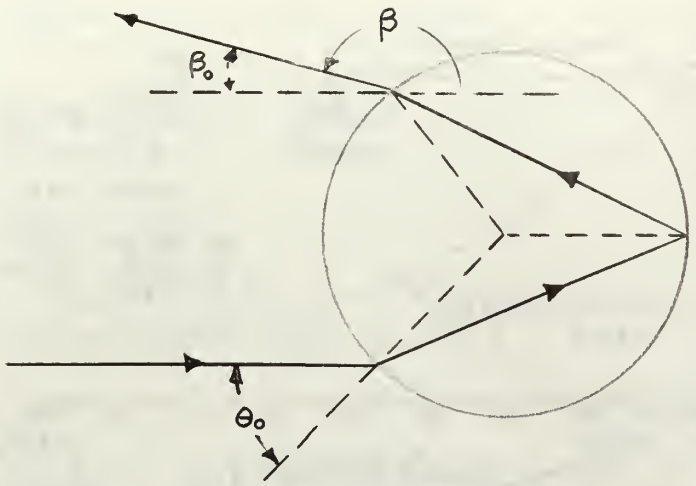

Figure 4.2

Stationary ray

Figure 4.3 illustrates the relationship between emergent angle β and incident angle θ_0 for a sphere of dielectric constant equal to 2.56 as given by Kawano. [5].

It is evident from Figure 4.3 that the minimum outgoing angle β min may be determined by setting $d\beta/d\theta_0$ equal to zero and solving for the resultant incident and refractive angles. This principle is an integral part of the derivation of the stationary ray contribution in Appendix I. The complexity of this derivation is not required at this point, however, as the matter of principal concern is the location of the stationary ray.

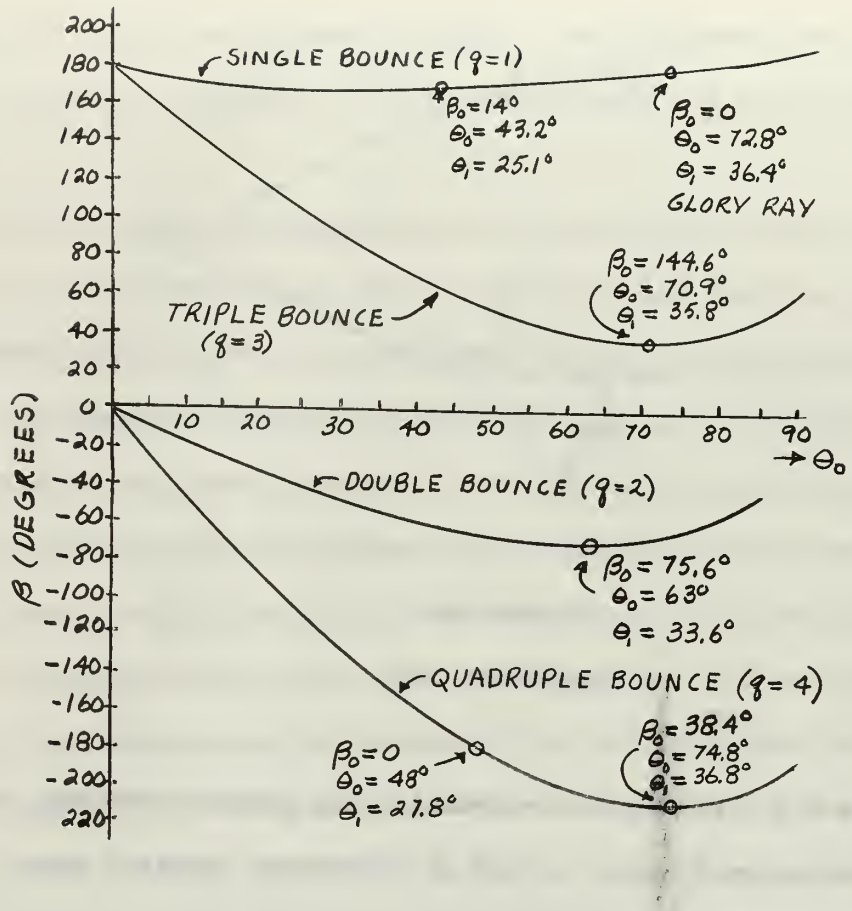

Figure 4.3

Emergent angle versus incident angle

The incident angle θ_{os} which results in the stationary ray may be found from Equations 4.1 and 4.2.

(4.1)

$$\beta = \pm \left[-2(q+1)\theta_1 + 2\theta_0 + q\pi \right]$$

(4.2) $$\sqrt{\epsilon_r}\sin\theta_1 = \sqrt{1}\sin\theta_0$$

$$\frac{d\beta}{d\theta_0} = -2q + \frac{d\theta_1}{d\theta_0} + 2 = 0$$

$$\frac{d\theta_1}{d\theta_0} = q + 1$$

(4.3) $$\theta_0 = \sin^{-1}(\sqrt{\epsilon_r}\sin\theta_1)$$

(4.4) $$\theta_{0s}\Big|_{\beta\,MIN} = \sin^{-1}\left[\frac{(q+1)^2 - \epsilon_r}{(q+1)^2 + 1}\right]^{1/2}$$

The single bounce stationary ray for a sphere of dielectric constant 2.56 occurs at an incident angle

$$\theta_{0s} = \sin^{-1}\left[\frac{4 - 2.56}{3}\right]^{1/2}$$

from which β_0 may now be calculated as 14°.

The dielectric constant required to place the stationary ray at ten degrees may be determined by plotting the resultant values of β_0 for numerous dielectric constants. Figure 4.4.

A dielectric constant of 2.85 was determined to be required from Equations 4.4, 4.2.

$$\theta_{0s} = \sin^{-1}\left[\frac{4 - 2.85}{3}\right]^{1/2} = 39^\circ$$

$$\sin\theta_0 = \sqrt{2.85}\sin\theta_1 \qquad \theta_1 = 22^\circ$$

$$\beta = -4(22) + 2(39) + 180 = 10^\circ$$

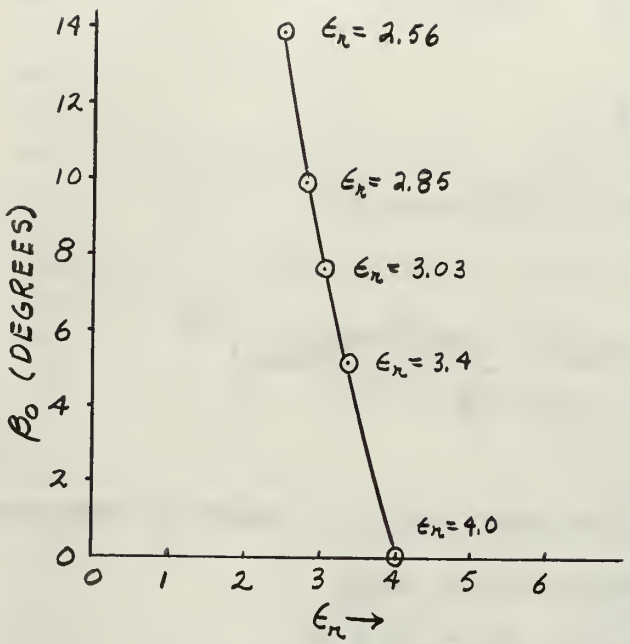

Figure 4.4

β_0 versus ϵ_r for a spherical lens

The foregoing considerations determined the shape, size and electrical properties of the lens. Experimentation consisted of the actual construction of three such lenses and measuring the radar backscatter patterns on the Micronetics outdoor backscatter range and in an anechoic chamber at the Naval Missile Test Center, Point Mugu. The following substances were chosen to provide stationary rays at bistatic angles less than ten degrees, greater than ten

degrees, and as nearly equal to ten degrees as available materials would permit.

Material:	Polystyrene	Napthalene	Nylon 66
Shape:	7" diameter sphere	7" diameter sphere	7" diameter sphere
ϵ_r	2.54	2.74	3.03
β_o	14°	11.6°	7.4°
f	10 GHz	10 GHz	10 GHz

Backscatter was measured at $\beta = 0^\circ$ (monostatic) and at every two degrees to $\beta = 20^\circ$. Measurements were taken every degree about the region of calculated β_o min.

5. Compound spherical lens of varied dielectric constant

Ray optics is utilized in developing a computer program for the return from a spherical lens of different front and rear surface radii, a "biradial spheroid". The method of analysis of the lens behavior does not follow previous work but is unique to this report. This analysis utilizes the authors' system of notation and definitions except where noted herein. Individual rays are traced through the lens by the application of Snell's Law. The appropriate transmission and reflection coefficients are developed and applied to obtain the emergent amplitude. The path phase length and associated phase shifts are determined to ascertain the phase of the emergent ray. The face of the lens is then divided into a large number of equal incremental areas with an incident ray entering each incremental area, a portion of the energy being reflected from that area, and a portion being refracted and ultimately re-radiated from some other incremental area. Each of these incremental areas is then considered to be a point source radiator of a selected radiation pattern. The far field is then determined from the summation of the E field resulting from each elemental radiator.

The foregoing calculations are accomplished in a program developed for the CDC 1604 computer. The results of this computer program are then compared to test data obtained from full scale models constructed of polystyrene, nylon, lucite, and napthalene.

The need for spherical symmetry, previously noted, again dictates the general shape of the lens. The radius, R_2 of the rear surface as shown in Figure 5.1 is now varied as is the dielectric constant. The computer program to provide the far field due to backscatter from an incident plane wave is developed as follows:

Equations of lens

The equation of the front surface of the lens is

(5.1)
$$(U-b)^2+V^2=R_1^2$$

and that for the rear surface

(5.2)
$$(U-b)^2+V^2=R_2^2$$

These surfaces extend only to their joint intersection as shown in Figure 5.2. The lens is a figure of revolution about the U axis.

Ray path equations

The incident ray enters the lens from the left parallel to the U axis. The geometry of the lens provides symmetrical backscatter for rays incident from approximately 115° to 235° (angles measured counter clock wise from the U axis). For aspect angles greater than these, some portion of the radiation strikes the outside rear surface as shown in Figure 5.1.

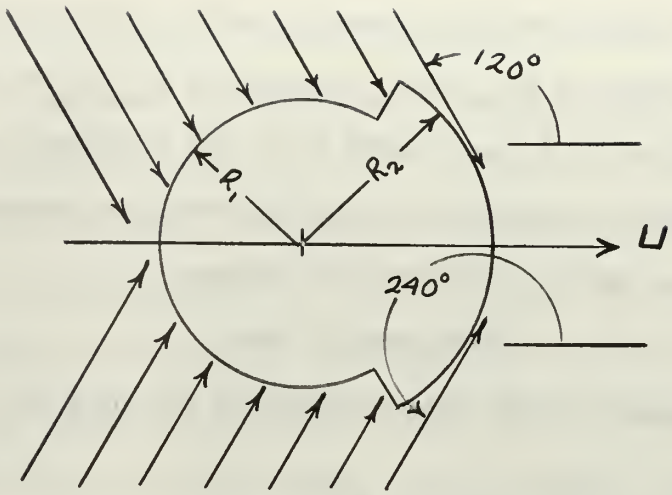

Figure 5.1

Maximum aspect angles

Lens symmetry also allows consideration of only those rays spaced from $V=0$ to $V=R_1$.

The manner of selection of V_1 , which is the entering argument for this computation, is discussed on page 45.

The refracted, reflected and transmitted ray paths are diagrammed in Figure 5.2. The parameters describing these paths are obtained as follows:

From Equation (5.1)

(5.3) $$U_1 = R_1 - [R_1^2 - V_1^2]^{1/2}$$

(5.4) $$m_1 = \frac{dV_1}{dU_1} = \frac{R_1 - U_1}{V_1}$$

(5.5) $$\lambda = -\tan^{-1}\left[\frac{V_1}{U_1 - R_1}\right]$$

(5.6)

$$\lambda' = \sin^{-1}\left[\frac{\sin\lambda}{\eta}\right]$$ from Snell's Law

η = index of refraction of the lens material

The slope

(5.7)

$$b_1 = \tan\left[\tan^{-1}\left(\frac{-1}{m_1}\right) + \lambda'\right]$$

and the line of slope b_1 is defined by

$$V - V_1 = b_1[U - U_1]$$

The point of ray intersection with the rear surface (surface #2) is determined by

(5.8) $$V_2 = b_1(U_2 - U_1) + V_1$$

$$V_2^2 = [b_1(U_2 - U_1)]^2 + 2V_1 b_1(U_2 - U_1) + V_1^2$$

$$(U_2 - b)^2 = R_2^2 - V_2^2$$

$$U_2^2 - 2U_2 b + b^2 = R_2^2 - [b_1(U_2 - U_1)]^2 - 2V_1 b_1(U_2 - U_1) - V_1^2$$

$$U_2^2[1 + b_1^2] + U_2[-2b - 2b_1^2 U_1 + 2V_1 b_1] + [b^2 - R_2^2 + b_1^2 V_1^2 - 2V_1 b_1 U_1 + V_1^2] = 0$$

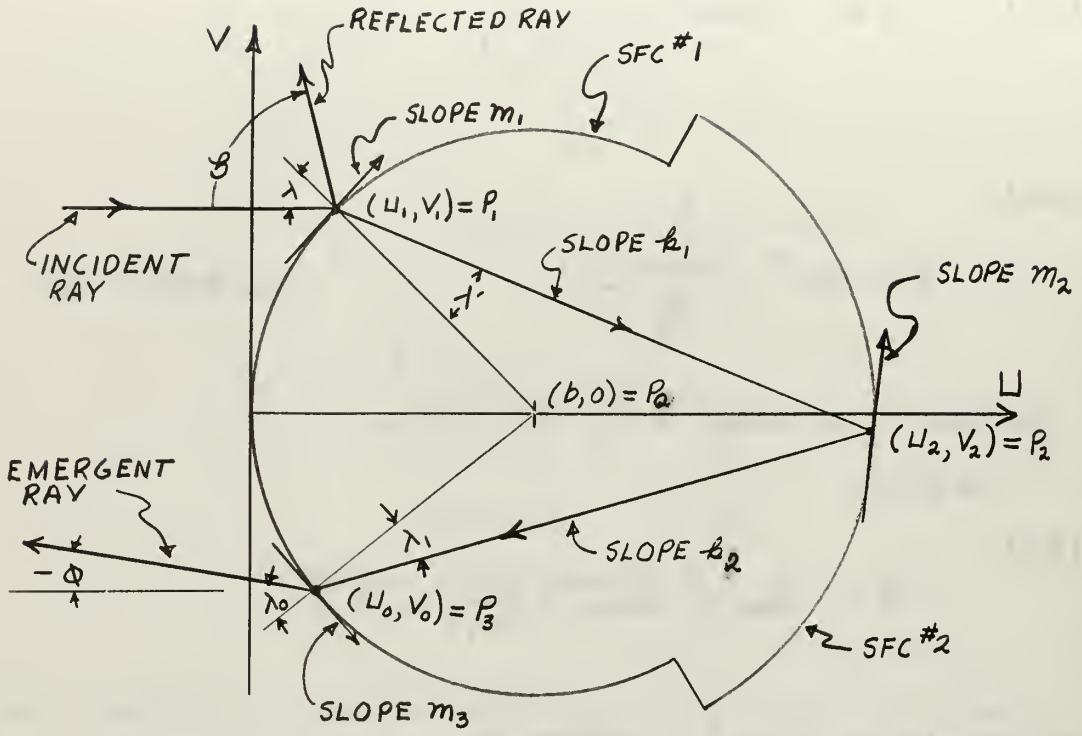

Figure 5.2

Internal ray paths

(5.9) $$U_2 = \frac{-B + [B^2 - 4A\Gamma]^{1/2}}{2A}$$ where

(5.10) $$A = 1 + k_1^2$$

(5.11) $$B = -2b - 2k_1^2 U_1 + 2V_1 k_1$$

(5.12) $$\Gamma = b^2 - R_2^2 + k_1^2 V_1^2 - 2V_1 k_1 U_1 + V_1^2$$

thus

(5.8) $$V_2 = b_1 [U_2 - U_1] + V_1$$

The angle of incidence of the ray at the rear surface is equal to the angle of reflection, therefore

(5.13) $$m_2 = \frac{dV_2}{dU_2} = \frac{b - U_2}{V_2}$$

(5.14) $$b_2 = \tan [2 \tan^{-1} m_2 - \tan^{-1} b_1]$$

The equation of the reflected internal ray is then expressed as

(5.15) $$V_0 = b_2 [U_0 - U_2] + V_2$$

The point of intersection of this ray with the front surface is determined as follows

$$V_0^2 = [b_2 (U_0 - U_2)]^2 + 2V_2 b_2 (U_0 - U_2) + V_2^2$$

$$(U_0 - R_1)^2 = R_1^2 - V_0^2$$

$$U_0^2 (1 + b_2^2) + U_0 [-2R_1 - 2 b_2^2 U_2 + 2 V_2 b_2]$$
$$+ [b_2^2 U_2^2 - 2 V_2 b_2 U_2 + V_2^2] = 0$$

(5.16) $$U_0 = \frac{-B_1 - [B_1^2 - 4A_1\Gamma_1]^{1/2}}{2A_1}$$

(5.17) $$A_1 = 1 + b_2^2$$

(5.18) $$B_1 = -2R_1 - 2b_2U_2 + 2V_2b_2$$

(5.19) $$\Gamma_1 = b_2^2U_2^2 - 2V_2b_2U_2 + V_2^2$$

The range of dielectrics considered $\sqrt{2} < \eta < 2$ and the spherical geometry of the lens limit the values of V_0 to $V_0 \leq 0$ for $V_1 \geq 0$.

$\lambda' = \lambda_1$ and $\lambda_0 = \lambda$ as triangles P_0, P_1, P_2 and P_0, P_3, P_2 are congruent. Figure 5.2

(5.20) $$m_3 = \frac{R_1 - U_0}{V_0}$$

(5.21) $$\phi = \tan^{-1}[m_3] - \lambda + 90^\circ$$

The sign of ϕ is negative when the ray emerges so as to intersect the U axis as shown in Figure 5.2.

The position (U_0, V_0) and angle ϕ of emergence for a transmitted ray that enters parallel to the U axis at point (U_1, V_1) have been determined.

The position of reflection from Figure 5.2 is (U_1, V_1) and, as the angle of incidence equals the angle of reflection

(5.22)
$$\gamma = 2\lambda$$

The angle γ is always positive $0 \leq \gamma \leq 180^\circ$ as only rays entering parallel to and above the U axis are considered. Those reflections for $\gamma \geq 90^\circ$ are not considered as they do not contribute to the backscattered field in the region of interest.

Ray spacing

The spacing of incoming rays will now be determined.

Figure 5.3 represents the projection of the front surface of the lens onto a plane perpendicular to the U axis. The plane E - M wave is considered to be incident perpendicularly to this plane (x, y plane). The circle of radius R is now divided into N equal area rings as shown in Figure 5.3.

(5.23)
$$r(i) = R_1 \sqrt{\frac{i}{N}} \qquad i = 1 \text{ to } N$$

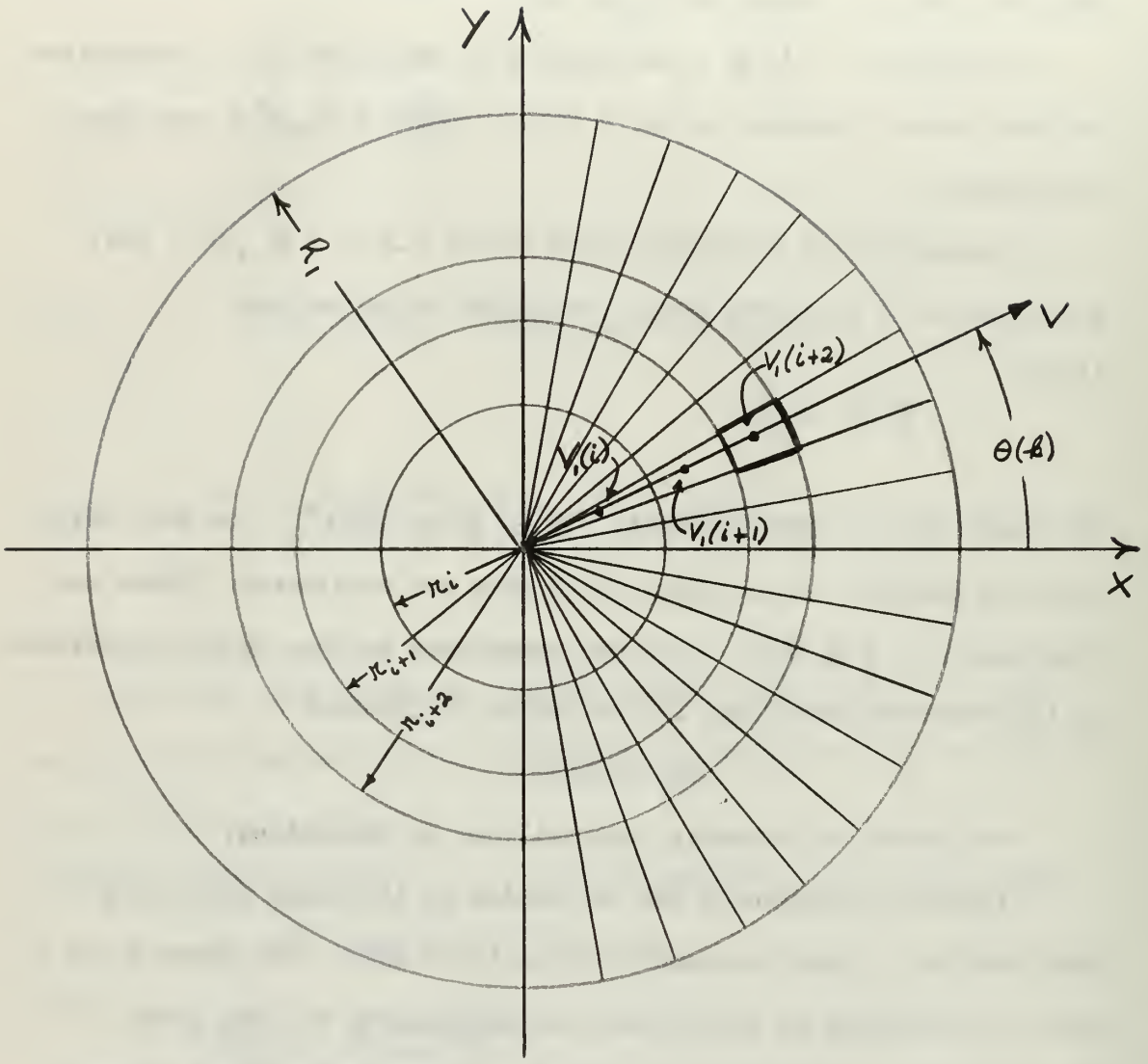

Figure 5.3

Projection of lens face onto x, y plane

Each ray is then centered in the associated incremental area by setting

(5.24) $$V_1(i) = \frac{r(i-1) + r(i)}{2} \qquad \text{where } r(0) \equiv 0$$

The V axis is now swept over one half of the lens face by setting

(5.25) $$\theta(k) = -92.5 + 5k$$

$$k = 1 \text{ to } 36$$

Each ray entering the lens represents an equal increment of energy of the incident wave. It is necessary to rotate the V axis over only one half of the lens face due to the symmetry of the lens. For ease of computation, the transmitted rays emerging in the positive X half plane are considered.

Transmission coefficients

Transmission coefficients are developed considering the x, y plane to be illuminated by a plane E - M wave with the E field (E_i) parallel to the X axis as shown in Figure 5.4. This polarization represents vertical polarization. The plane of incidence is perpendicular to the x, y plane and contains the V axis.

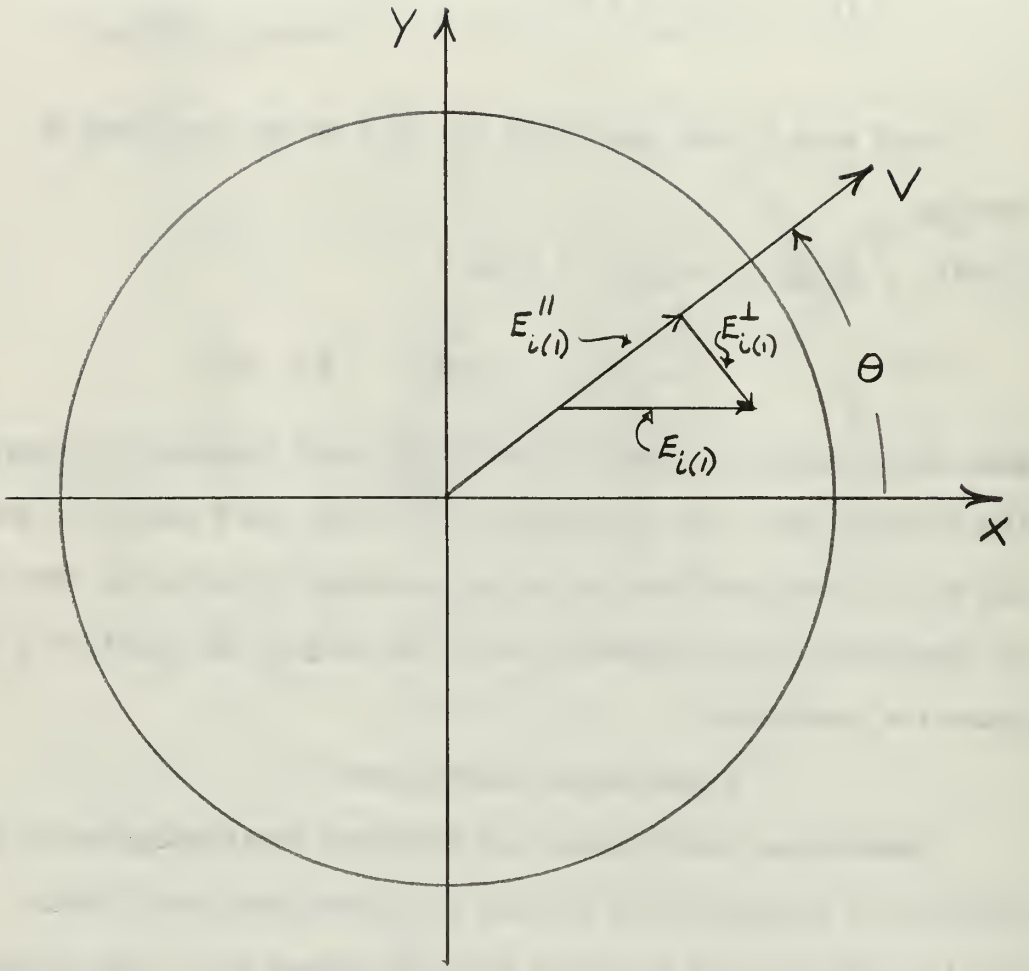

Figure 5.4

Vector components of incident radiation (face on view)

$E^{\parallel}_{i(1)}$ ≡ The component of the electric field parallel to the V axis incident upon the lens.

$E^{\perp}_{i(1)}$ ≡ The component of the electric field perpendicular to the V axis incident upon the lens.

$$E^{\parallel}_{i(1)} = E_{i(1)} \cos\theta$$

$$E^{\perp}_{i(1)} = E_{i(1)} \sin\theta$$

$E^{(\parallel,\perp)}_{t(1-2)}$ ≡ The magnitude of the electric field transmitted into the lens.

$$T^{\parallel}_{12} \equiv \frac{E^{\parallel}_{t(2)}}{E^{\parallel}_{i(1)}} \qquad T^{\perp}_{12} \equiv \frac{E^{\perp}_{t(2)}}{E^{\perp}_{i(1)}}$$

$$E^{\parallel}_{t(1-2)} = E_{i(1)} T^{\parallel}_{12} \cos\theta$$

$$E^{\perp}_{t(1-2)} = E_{i(1)} T^{\perp}_{12} \sin\theta$$

$E_{i(2)}$ ≡ The magnitude of the electric field incident upon the boundary (lens to air).

The reflection coefficient of the metal cap on the back surface is assumed to be unity. Therefore

$$\left| E_{i(2)} \right| = \left| E_{t(1-2)} \right|$$

The 180° phase shift at reflection will be taken into account later. The absolute value signs are deleted for convenience.

$E^{(\parallel,\perp)}_{t(2-1)}$ ≡ The magnitude of the electric field transmitted from lens to air.

$$E''_{t(2-1)} = E''_{i(2)} T''_{21} = E''_{t(1-2)} T''_{21} = E_{i(1)} T''_{12} T''_{21} \cos\theta$$

$$E^{\perp}_{t(2-1)} = E^{\perp}_{i(2)} T^{\perp}_{21} = E^{\perp}_{t(1-2)} T^{\perp}_{21} = E_{i(1)} T^{\perp}_{12} T^{\perp}_{21} \sin\theta$$

Equations 5.26, 5.27, 5.28, 5.29, 5.33, and 5.34 are given by Jenkins and White. [4].

(5.26) $$T''_{12} = \frac{2 \sin\lambda' \cos\lambda}{\sin(\lambda+\lambda') \cos(\lambda-\lambda')}$$

(5.27) $$T^{\perp}_{12} = \frac{2 \sin\lambda' \cos\lambda}{\sin(\lambda+\lambda')}$$

(5.28) $$T''_{21} = \frac{2 \sin\lambda \cos\lambda'}{\sin(\lambda'+\lambda) \cos(\lambda'-\lambda)}$$

(5.29) $$T^{\perp}_{21} = \frac{2 \sin\lambda \cos\lambda'}{\sin(\lambda+\lambda')}$$

(5.30) $$\tau'' \equiv T''_{12} T''_{21}$$

(5.31) $$\tau^{\perp} \equiv T^{\perp}_{12} T^{\perp}_{21}$$

λ and λ' are the angles of incidence and refraction as appropriate. The direct interchange of λ and λ' between T_{12} and T_{21} is possible due to the fact that $\lambda_1 = \lambda'$ and $\lambda_0 = \lambda$ as noted previously.

The magnitude of the emergent E field may now be determined. Only the vertically polarized component is considered (component parallel to the X axis). Defining E_T as this component

$$E_T = E''_{t(2-1)} \cos\theta + E^{\perp}_{t(2-1)} \sin\theta$$

$$= E_{i(1)} \tau'' \cos^2\theta + E_{i(1)} \tau^{\perp} \sin^2\theta$$

Normalizing $E_{i(1)}$ to unity results in

(5.32) $$E_T = \tau'' \cos^2\theta + \tau^{\perp} \sin^2\theta$$

Reflection coefficients

The parallel and perpendicular reflection coefficients are

(5.33) $$R'' = \frac{\tan(\lambda - \lambda')}{\tan(\lambda + \lambda')}$$

(5.34) $$R^{\perp} = -\frac{\sin(\lambda - \lambda')}{\sin(\lambda + \lambda')}$$

$E_R^{(\parallel,\perp)}$ The component of the reflected electric field at the lens face parallel or perpendicular to the V axis

$$E_R'' = E_{i(1)}'' R'' = E_{i(1)} R'' \cos\theta$$

$$E_R^{\perp} = E_{i(1)}^{\perp} R^{\perp} = E_{i(1)} R^{\perp} \sin\theta$$

Defining the desired vertically polarized component as E_R

$$E_R = E_R'' \cos\theta + E_R^{\perp} \sin\theta$$

$$= E_{i(1)} R'' \cos^2\theta + E_{i(1)} R^{\perp} \sin^2\theta$$

Normalizing $E_{i(1)} = 1$

(5.35) $$E_R = R'' \cos^2\theta + R^{\perp} \sin^2\theta$$

Internal losses

The resultant electric field of the transmitted ray must be modified to take into account the attenuation due to lossy dielectric medium. The attenuation of the wave as it propagates through the lens material may be expressed as $e^{-\alpha z}$ where α is the attenuation constant and z is the distance traveled. For dielectrics with $\tan\delta << 1$ the attenuation constant may be approximated by

$$\alpha \approx \frac{\pi}{\lambda_{MEDIUM}} \tan\delta = \frac{\pi}{\lambda_{air}} \eta \tan\delta$$

as given by Ramo and Whinnery. [6].

Where $\tan \delta \equiv \frac{\epsilon''}{\epsilon'}$ (loss tangent)

Let

(5.36) $F = e^{-\frac{\pi}{\lambda_{AIR}} \tan \delta (LM)}$

where LM is the electrical path length in the medium (see Equation 5.42) and λair is the wave length of the radiation.

Electric far field summation

Thus far we have found the positions of the transmitted and reflected rays with respect to the x, y plane at the face of the lens and the magnitudes of the transmitted and reflected electric fields at these positions.

The total E field in the direction of the vector $\vec{A}$ (representing bistatic direction) will be the vector sum of all the elementary radiators formed by the dispersion of the rays emerging from and reflected from the lens face. Rays that are internally reflected more than once are not considered. Examination of the magnitudes of the transmission coefficients indicates that these multiple bounce rays make only minor contributions to the total electric field.

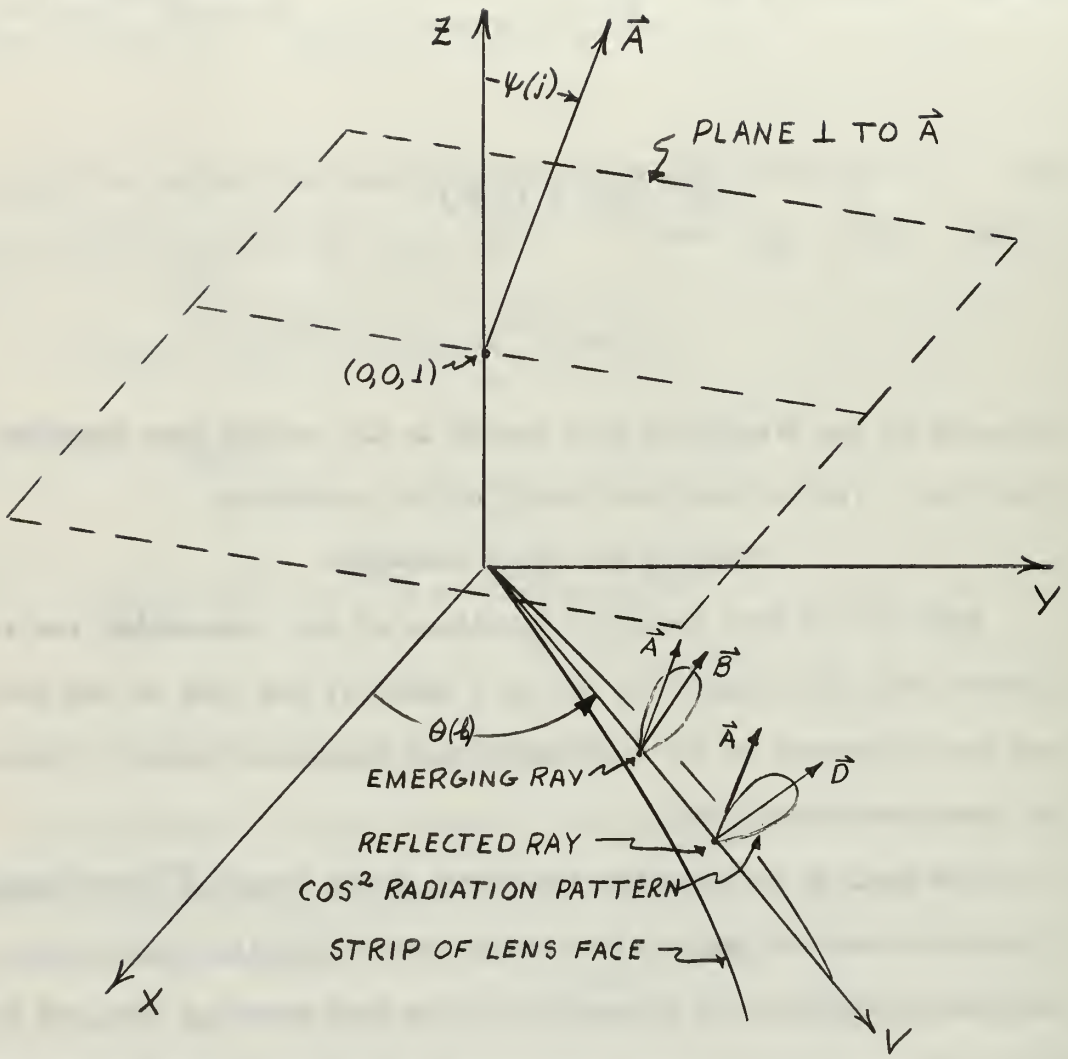

Figure 5.5

Co-ord system for summing far field contribution of each emerging and reflected ray

We assume that each elemental radiator has a $\cos^2$ pattern.

For arbitrary $\theta(b)$ we compute the following:

Computer symbol	Text variable	Definitions
RHO2 (I)	$V_1(i)$	position of entering ray, perpendicular distance from z axis.
z ETA (I)	$\gamma(i)$	the angle between a reflected ray and the z axis.
REFV (I)	R''	see Equation 5.33.
REFH (I)	$R^{\perp}$	see Equation 5.34.
TRAH12 (I)	$T_{12}^{\perp}$	see Equation 5.27.
TRAH21 (I)	$T_{21}^{\perp}$	see Equation 5.29.
TRAV12 (I)	T_{12}''	see Equation 5.26.
TRAV21 (I)	T_{21}''	see Equation 5.28.
TAUH (I)	$\tau^{\perp}$	see Equation 5.31.
TAUV (I)	τ''	see Equation 5.30.
XLA (I)	LA	incident ray path length in air see Equation 5.41.
XLM (I)	LM	ray path length within lens see Equation 5.42.
RHOI (I)	$\lvert V_0(i)\rvert$	position of emerging ray, perpendicular distance from z axis.
FAC (I)	F	attenuation of the magnitude of the transmitted electric field due to lossy dielectric see Equation 5.36.
XO (I)	$-U_0(i)$	Z co-ordinate of emerging ray
PHI (I)	$\phi(i)$	the angle that the emerging ray makes with the z axis

For arbitrary $\psi(j)$, $\theta(k)$, we compute the following:

CGAM	$\cos\gamma$	Gamma is the angle between the vector representing bistatic direction and the vector representing direction of the emerging ray.
CBET	$\cos\beta$	Beta is the angle between the vector representing bistatic direction and the vector representing direction of the reflected ray.
D	D	the perpendicular distance from point of ray emergence to a reference plane containing the point (0, 0, 1) and perpendicular to the bistatic direction.
DR	DR	the perpendicular distance from point of ray reflection on lens face to a reference plane containing the point (0, 0, 1) and perpendicular to the bistatic direction.
PHASE	ξ_e	phase of elemental radiator (emergent ray) at reference plane perpendicular to bistatic direction.
PHASR	ξ_r	phase of elemental radiator (reflected ray) at reference plane perpendicular to bistatic direction.

Referring to Figure 5.5, the following equations are developed for use in computing $\cos\gamma$, $\cos\beta$, D, DR, ξ_e , and ξ_r .

$\frac{\vec{A}}{|\vec{A}|}$ is a unit vector representing the bistatic direction in which we want to determine the magnitude of the total backscattered E field. $\vec{A}$ always lies in the z , y plane and ψ is the angle between the z axis and $\vec{A}$.

$$\frac{\vec{A}}{|\vec{A}|} = 0\,\vec{i} + \sin\psi(j)\,\vec{j} + \cos\psi(j)\,\vec{k}$$

$\vec{i}$, $\vec{j}$ and $\vec{k}$ are unit vectors in the x, y, z co-ordinate system shown in Figure 5.5.

$\frac{\vec{B}}{|\vec{B}|}$ is a unit vector in the direction of the emergent ray.

$$\frac{\vec{B}}{|\vec{B}|} = \sin\phi(i)\cos\theta(k)\,\vec{i} + \sin\phi(i)\sin\theta(k)\,\vec{j} + \cos\phi(i)\,\vec{k}$$

(5.37)
$$\cos\gamma = \frac{\vec{A}}{|\vec{A}|} \cdot \frac{\vec{B}}{|\vec{B}|}$$
$$= 0 + \sin\psi(j)\sin\phi(i)\sin\theta(k) + \cos\psi(j)\cos\phi(i)$$

The sign of $\phi(i)$ changes from $+$ to $-$ as $V_1(i)$ approaches $V_1(i=N)$. This change of sign is detected in the computer program such that if

$$\phi < 0 \qquad \theta(k) = \theta(k) + \pi$$

This permits $\cos\gamma$ to be computed correctly for all $\phi(i)$.

$\frac{\vec{D}}{|\vec{D}|}$ is a unit vector in the direction of the ray reflected from the lens face.

$\mathcal{G}$ is the angle between the z axis and the reflected ray.

$$\frac{\vec{D}}{|\vec{D}|} = \sin\mathcal{G}(i)\cos\theta(k)\,\vec{i} + \sin\mathcal{G}(i)\sin\theta(k)\,\vec{j} + \cos\mathcal{G}(i)\,\vec{k}$$

(5.38)
$$\cos\beta = \frac{\vec{A}}{|\vec{A}|} \cdot \frac{\vec{D}}{|\vec{D}|}$$
$$= \sin\psi(j)\sin\mathcal{G}(i)\sin\theta(k) + \cos\psi(j)\cos\mathcal{G}(i)$$

The position at which a ray emerges from the lens is given by

$$X = |V_0(i)| \cos\theta(k)$$
$$Y = |V_0(i)| \sin\theta(k)$$
$$Z = -U_0(i)$$

(See Figures 5.5 and 5.2)

$\vec{C}$ is a vector from the point (0, 0, 1) to the point (x, y, z) at which the ray emerges

$$\vec{C} = [|V_0(i)| \cos\theta(k) - 0]\vec{i} + [|V_0(i)| \sin\theta(k) - 0]\vec{j} + [-U_0(i) - 1]\vec{k}$$

Thus

(5.39) $$D = \left| \frac{\vec{A}}{|\vec{A}|} \cdot \vec{C} \right|$$

$$= \left| |V_0(i)| \sin\theta(k) \sin\psi(j) + \cos\psi(j)\left[-U_0(i) - 1\right] \right|$$

The reason for choosing the point (0, 0, 1) to lie in the reference plane perpendicular to $\vec{A}$ is to insure that the reference plane does not intersect the lens for any $\psi(j)$ considered.

The position at which a ray is reflected from the lens face is given by

$$X = V_1(i) \cos\theta(k)$$
$$Y = V_1(i) \sin\theta(k)$$
$$Z = -U_1(i)$$

(See Figures 5.5 and 5.2)

$\vec{F}$ is a vector from the point (0, 0, 1) to the point (x, y, z) at which the ray is reflected from the lens face.

$$\vec{F} = [V_1(i) \cos\theta(k) - 0]\vec{i} + [V_1(i) \sin\theta(k) - 0]\vec{j} + [-U_1(i) - 1]\vec{k}$$

Thus

$$(5.40)\qquad DR = \left| \frac{\vec{A}}{|\vec{A}|} \cdot \vec{F} \right|$$

$$= \left| V_1(i) \sin\theta(b) \sin\psi(j) + \cos\psi(j)\left[-U_1(i) - 1\right] \right|$$

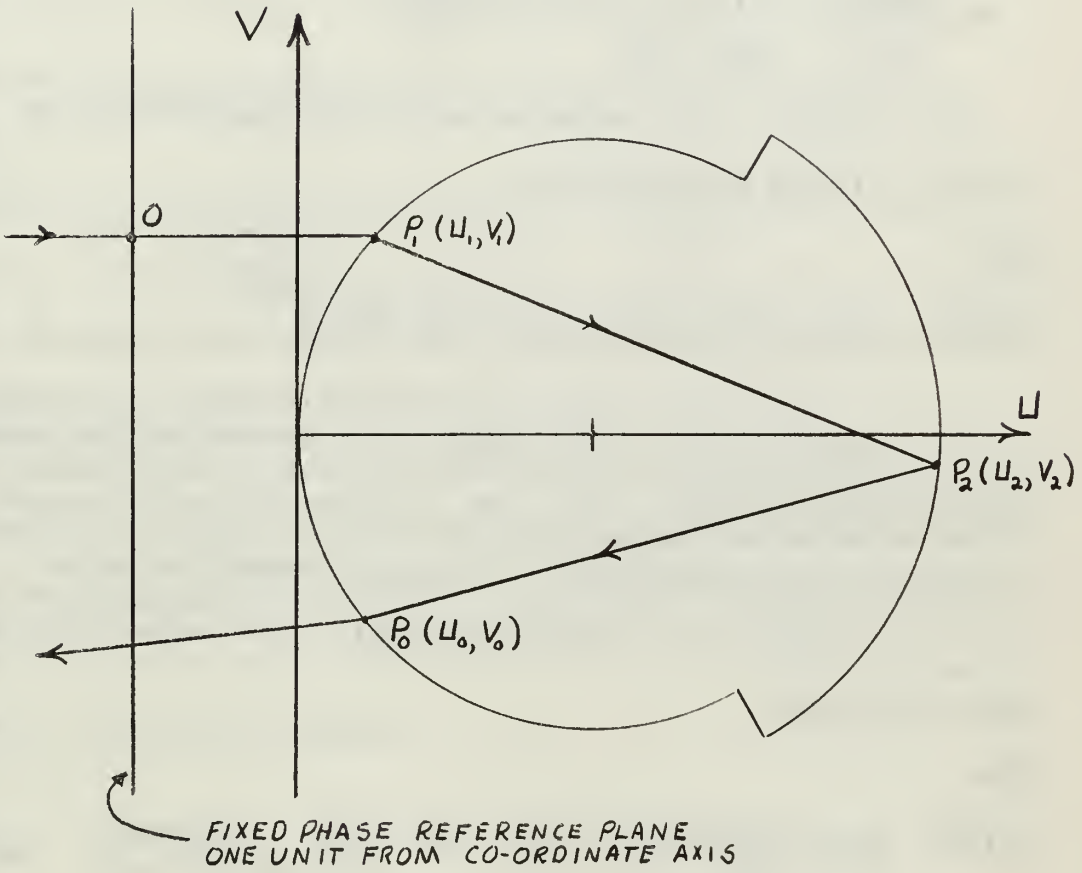

Figure 5.6

Ray paths

Referring to Figure 5.6, the following equations are developed for use in determining the relative phases of the elemental radiators for arbitrary bistatic angle (Ψ).

(5.41) $\overline{OP_1} = LA = U_1(i) + 1$

$\overline{P_1 P_2 P_0}$ = Geometric path length in the lens

$\overline{P_1 P_2 P_0} = 2\left[(U_2 - U_1)^2 + (V_1 - V_2)^2\right]^{1/2}$

SINCE $\overline{P_1 P_2} = \overline{P_2 P_0}$

The electrical path length in the lens is lengthened by the factor η (index of refraction).

Thus

(5.42) $LM = 2\eta\left[(U_2 - U_1)^2 + (V_1 - V_2)^2\right]^{1/2}$

The total electrical path length of the transmitted ray measured from the fixed reference plane shown in Figure 5.6 to the movable reference plane (perpendicular to $\vec{A}$ passing through the point (0, 0, 1), Figure 5.5) is given by LA+ LM + D. The units of LA, LM, and D are inches.

Thus

(5.43) $\xi_e = \frac{360 \times 2.54}{\lambda_{AIR}}\left[LA + LM + D\right]$ (DEGREES)

where λ air is defined as the wave length of the incident radiation in centimeters.

There would have been a factor of 180° in the expression for ξ_c to account for the phase shift upon internal reflection at the conducting cap, but the 180° is cancelled by the -180° phase shift introduced by the two caustics that each internal ray crosses.

The total electrical path length of the ray reflected at the lens face; measured from the fixed reference plane, shown in Figure 5.6, to the movable reference plane (perpendicular to $\vec{A}$ passing through the point (0, 0, 1), Figure 5.5), is given by LA+DR (inches). Thus

$$\xi_n = \frac{360 \times 2.54}{\lambda_{AIR}} [LA + DR] \quad (\text{DEGREES}) \tag{5.44}$$

The phase shifts introduced upon reflection at the lens face are accounted for in the reflection coefficients. ($R^{\parallel}$, $R^{\perp}$)

All necessary parameters have now been determined for the calculation of the magnitude and phase of the transverse component of the electric field of both the emergent ray and the reflected ray. Let

$$E = E_T F \cos^2 \gamma \tag{5.45}$$

$$E_{RT} = E_R \cos^2 \beta \tag{5.46}$$

The resultant normalized transverse electric field for a given bistatic angle, $\psi(j)$ is given by

(5.47) $$E(j)_{\text{RESULTANT}} = \sum_{i=1}^{N} \sum_{k=1}^{K} E e^{j\xi_e} + E_{RT} e^{j\xi_r}$$

$i = 1, N$ represents the spacing of the incident rays for each line of rays along the V axis.

$k = 1, K$ represents sweeping the lines of rays across the lens face

$$(i.e. \quad -90^\circ \leq \theta(k) \leq 90^\circ)$$

The locus of points given by $E(j)_{\text{RESULTANT}} = f(\psi(j))$ represents the cross section in the z , y plane of the backscattered electric far field for polarization with incident electric field parallel to the X axis (vertical polarization).

6. Results and conclusions

The computer program developed for the dielectric lens provided the data necessary to determine the normalized far E field as bi-static angle was varied from 0^{o} to 20^{o}. Programs were prepared for spheroidal and spherical lens of different dimensions, dielectric constants, and loss tangents. See Appendix II for a sample computer program.

Full scale models of these lenses were constructed and tested in an anechoic chamber. Some models were also tested on the outdoor Radar Backscatter Range at Micronetics, Inc. The data obtained, however, coincided with that of the anechoic chamber and is not presented separately.

The models were mounted on a styrofoam column and rotated through an angle of 180^{o}. The backscattered return was received and plotted by an automatic recorder. Prior to each test run, the background return from the chamber and styrofoam column was nulled and a calibration pattern was run on a standard flat plate. The return from the plate, which is 5.97 inches in diameter, is illustrated in Figure 6.6. The radar cross section of the plate is computed from

(6.1) $$\sigma_F = \frac{4\pi^2 A^2}{\lambda^2}$$

A = area

λ = wave length

and is equal to 4.7 square meters or 6.7 db above one square meter for

$$\lambda = 3 \text{ cm}$$

A composite graph of the test results for each lens is shown in Figures 6.1, 6.2, 6.3, 6.4, 6.5. It may be seen that the radar return for small bistatic angles is nearly constant over $\pm 60^{\circ}$ of azimuth. The non-uniform radar return for large bistatic angles is believed to be due to surface irregularities of the lens and slight variations of dielectric constant of the lens material.

The normalized E field from the computer program is plotted, versus bistatic angle in Figures 6.7, 6.8, 6.9, 6.10, 6.11. The radar return, averaged in azimuth, from the associated model is also plotted on the same figures for comparison. The monostatic (0°) radar return for the computed curve is set equal to the measured monostatic return for each lens.

The computed curves represent radar return as a function of bistatic angle for 0° azimuth.

The final results of this study are considered to be the plots of predicted normalized E field versus that actually measured, Figures 6.7-6.11.

From these results, it is concluded that:

(a). The stationary ray placement significantly alters the backscattered far E field. The pattern in Figure 6.8 for the nylon sphere, for which the stationary ray angle equals 7.6 ,

is considerably broadened in the principal peak region (0° to 10°) as compared to the other materials. The return for the napthalene and polystyrene with $\beta_o \approx 10^\circ$ and 14° respectively, is narrowed in the principal peak region, but the amplitude is relatively greater within the β_o region. This contribution is evident in both the calculated and measured fields.

(b). The use of geometric optics combined with selected radiation patterns provides valid predictions of the backscatter from a dielectric lens. The E fields predicted by the computer program compares closely with those measured as evidenced by Figures 6.7, 6.8, 6.9, 6.10, 6.11. With a given set of parameters such as dielectric constant, loss tangent, space available, pattern desired; it is felt that this program would provide the necessary data to design the desired lens.

(c). An approximation to the bistatic radar cross section of a lens can be made as follows:

(6.2) $$\sigma_{LENS}(\psi) \approx \sigma_F \left[\frac{E_n(\psi)}{NK} \right]^2$$

$\sigma_{LENS}(\psi)$ bistatic radar cross section of spheroidal lens for a given angle.

σ_F radar cross section of a circular flat plate of the same size as the lens cross section.

$E_n(\psi)$ resultant normalized transverse backscattered electric field for a given bistatic angle (as predicted by the computer program).

NK number of rays entering the lens.

In using this approximation, it is necessary to know the index of refraction and the loss tangent to a high degree of accuracy. Comparison of results computed by this method and measured data for the monostatic case is illustrated in Figure 6.12.

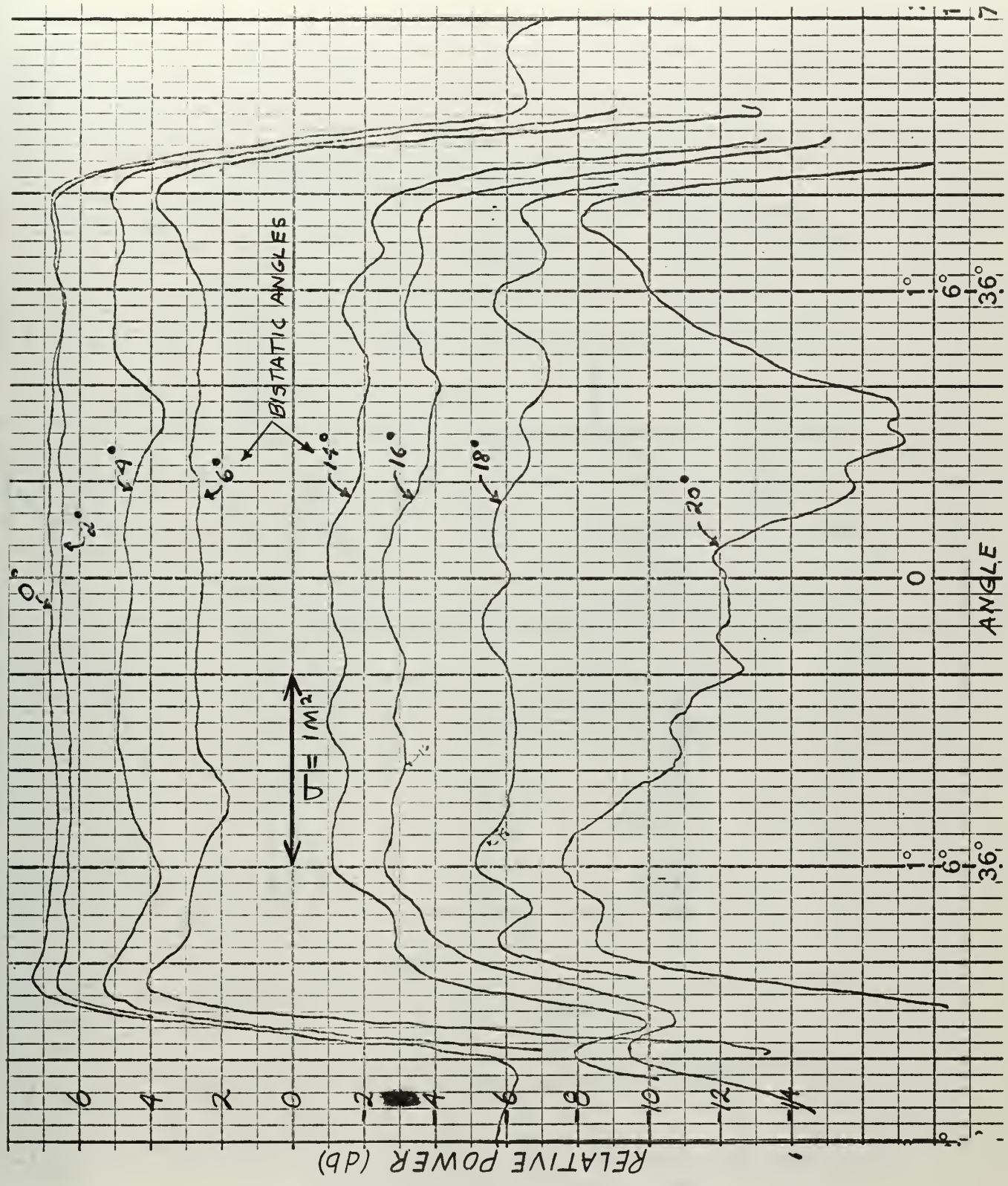

Figure 6.1

Measured radar return for napthalene sphere

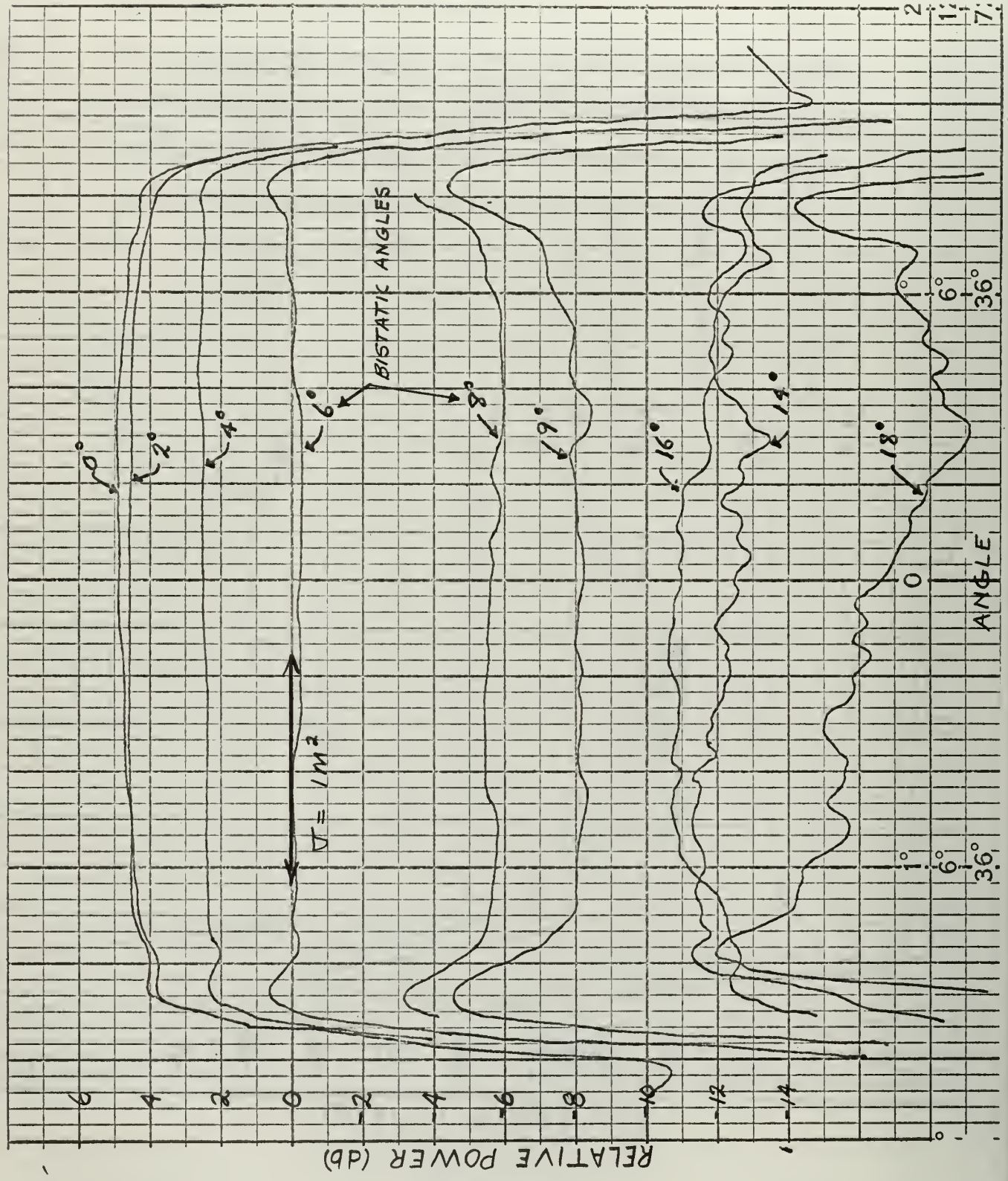

Figure 6.2

Measured radar return for a nylon sphere

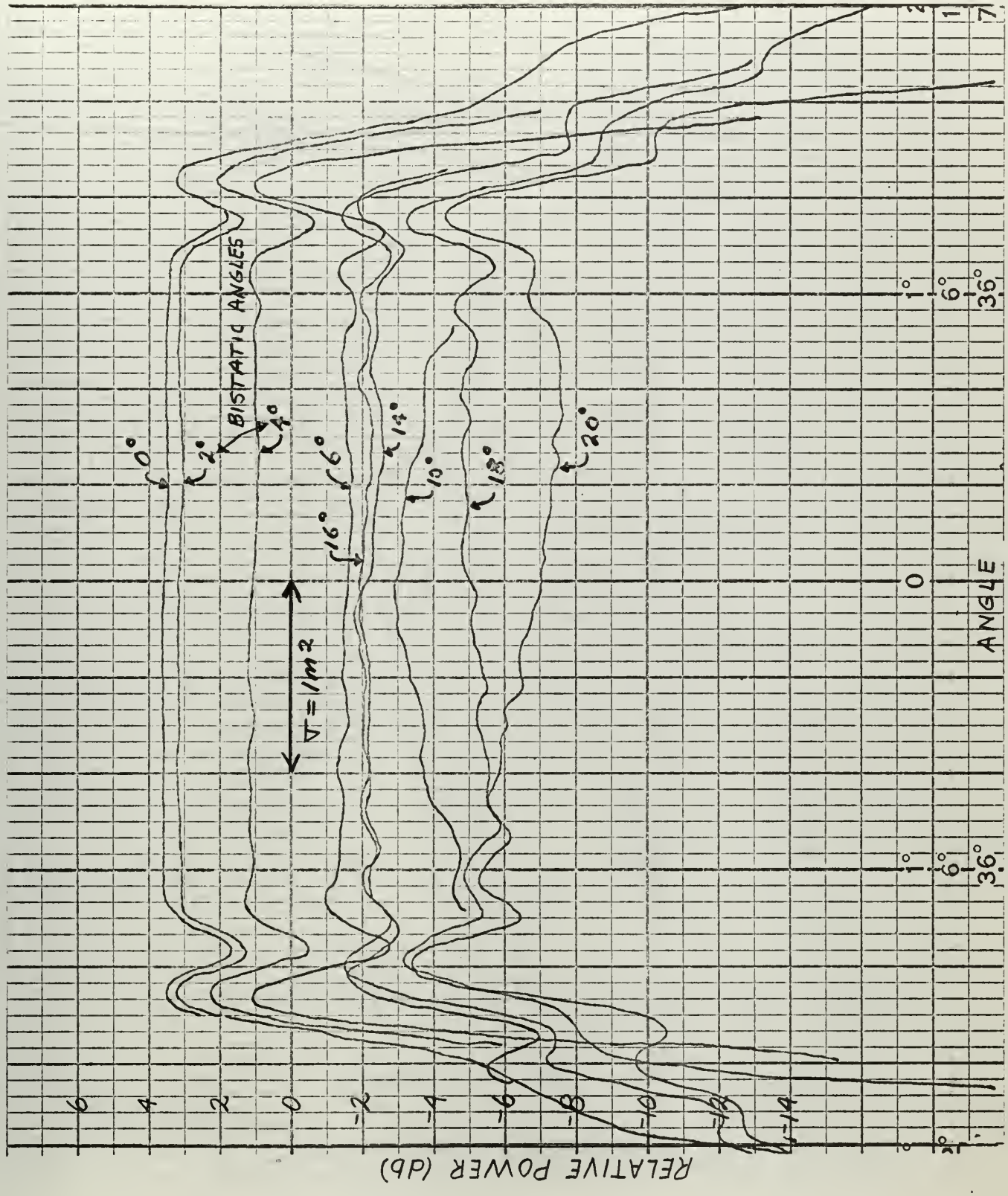

Figure 6.3

Measured radar return for a polystyrene sphere

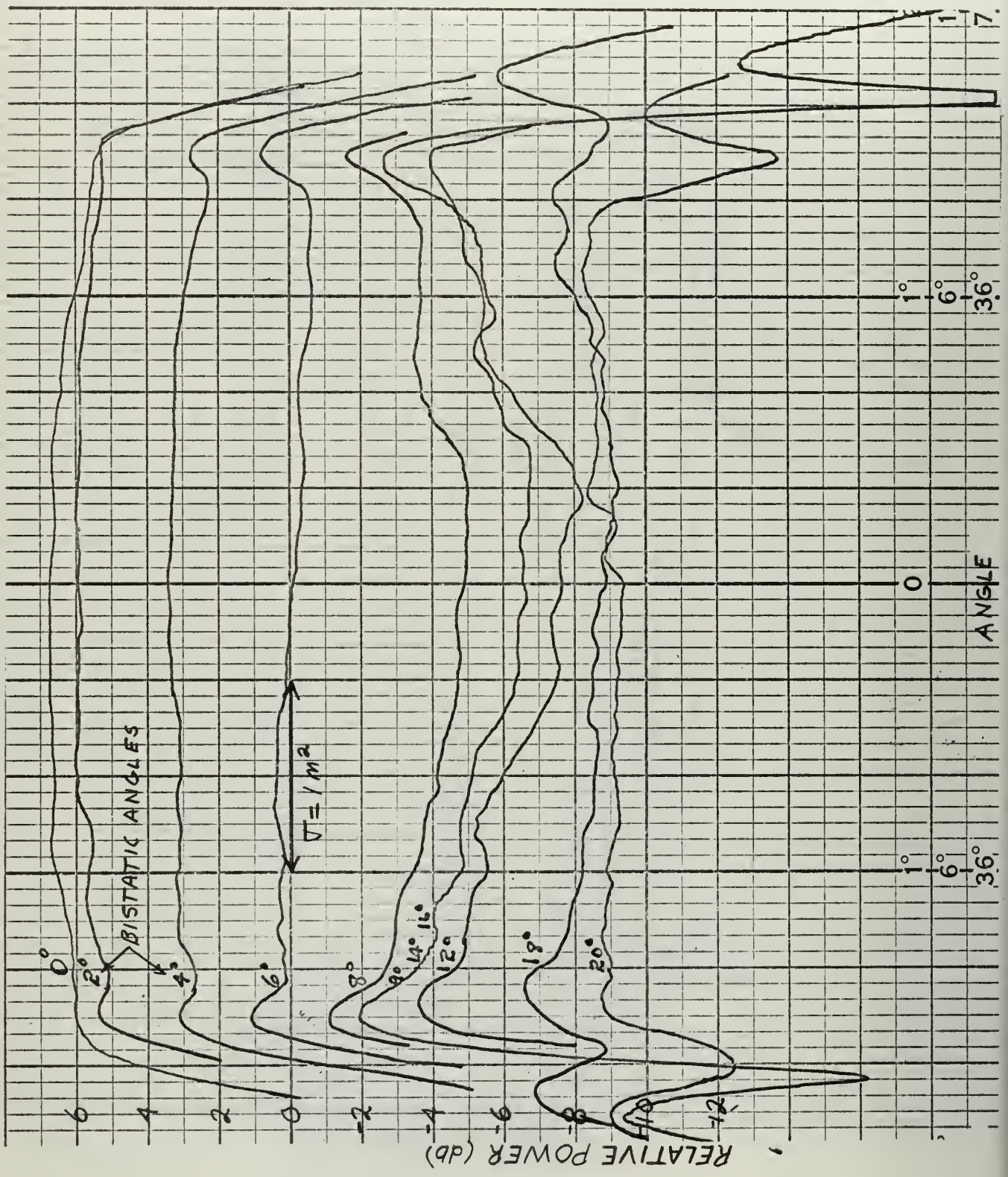

Figure 6.4

Measured radar return for lucite spheroid (R_2 3.83")

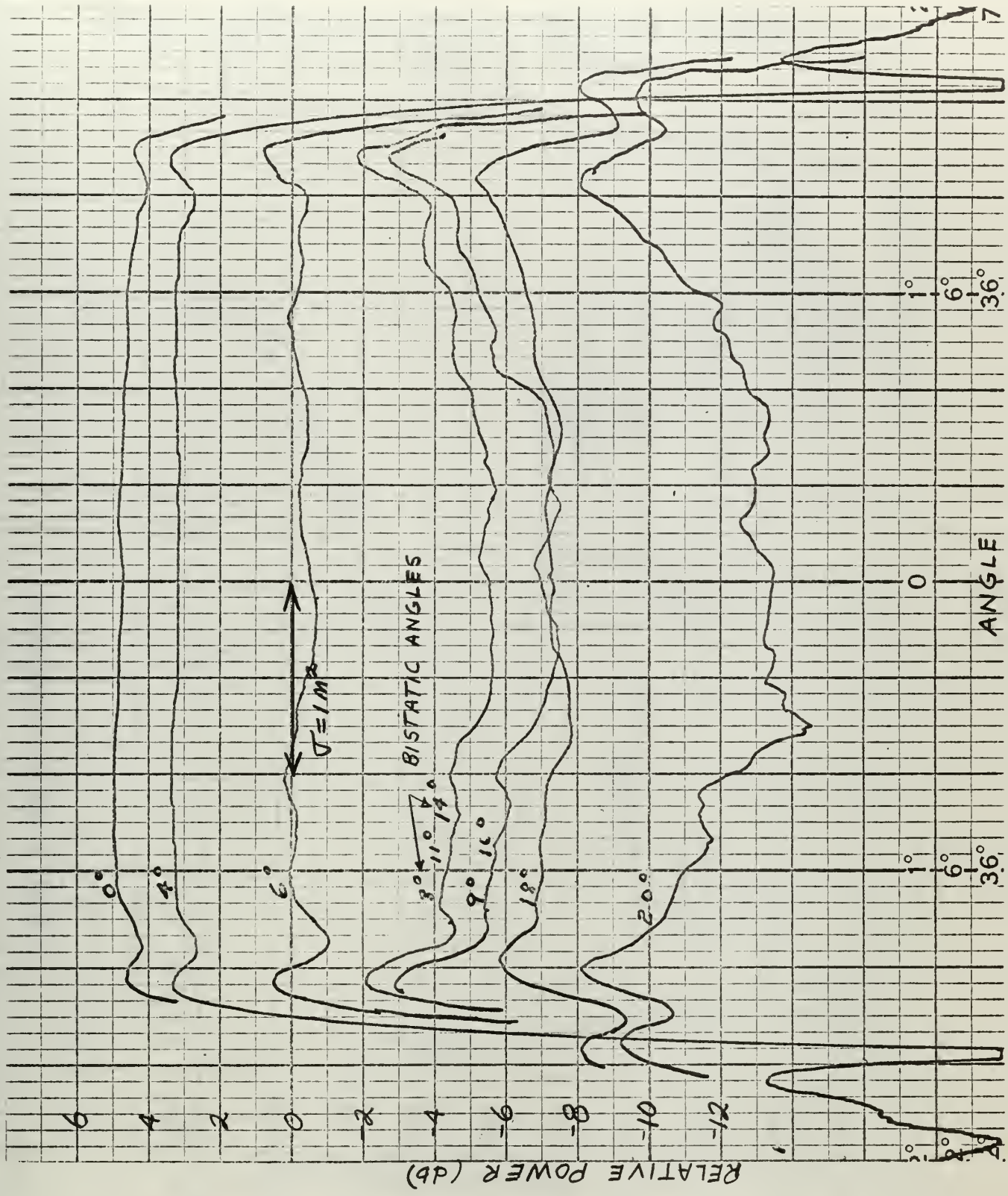

Figure 6.5

Measured radar return for lucite spheroid (R_2 3.7")

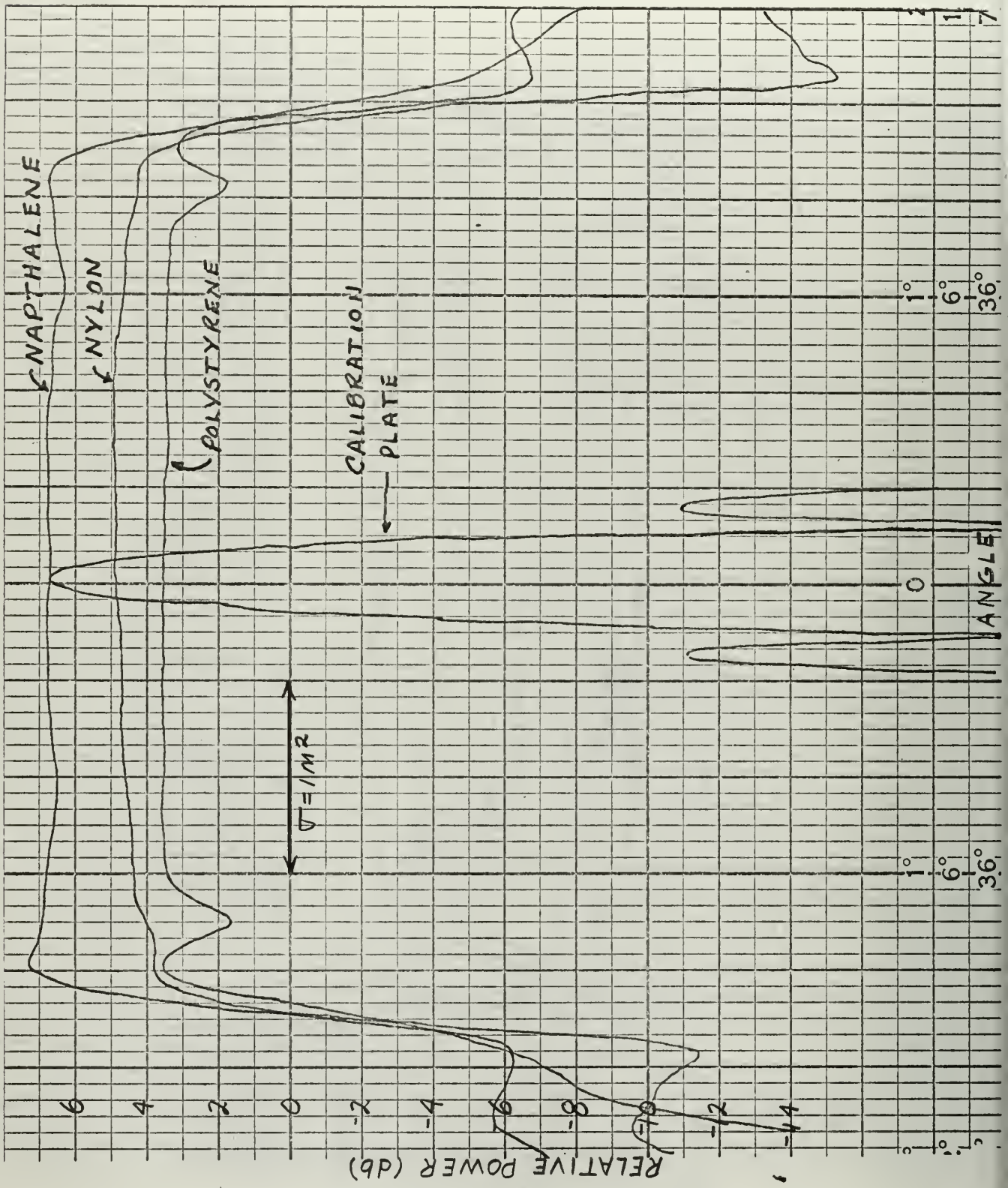

Figure 6.6

Monostatic radar return for napthalene, nylon, polystyrene sphere and flat plate

RADAR CROSS SECTION vs BISTATIC ANGLE FOR A NAPTHALENE SPHERE

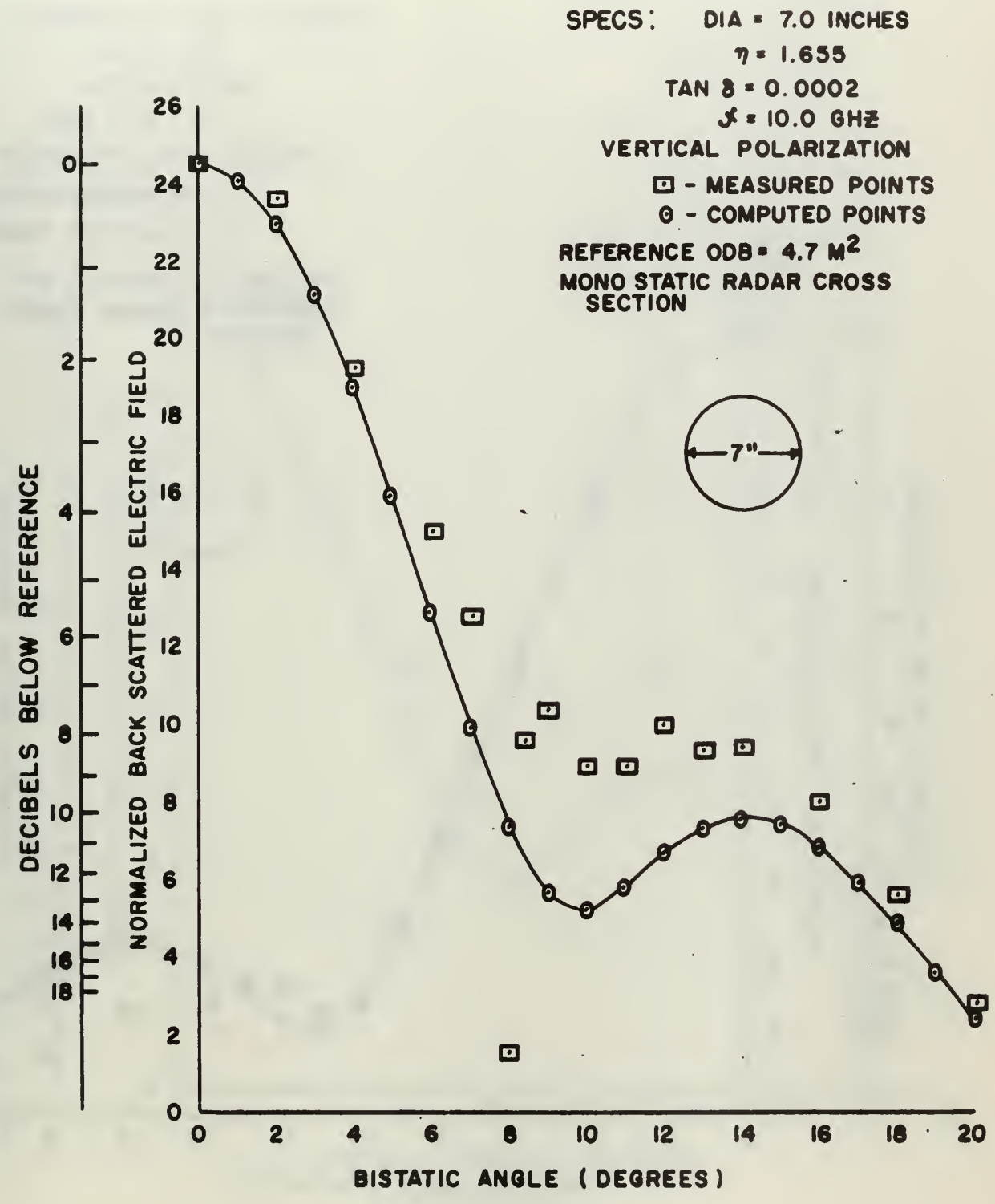

Figure 6.7

RADAR CROSS SECTION vs BISTATIC ANGLE FOR A NYLON SPHERE

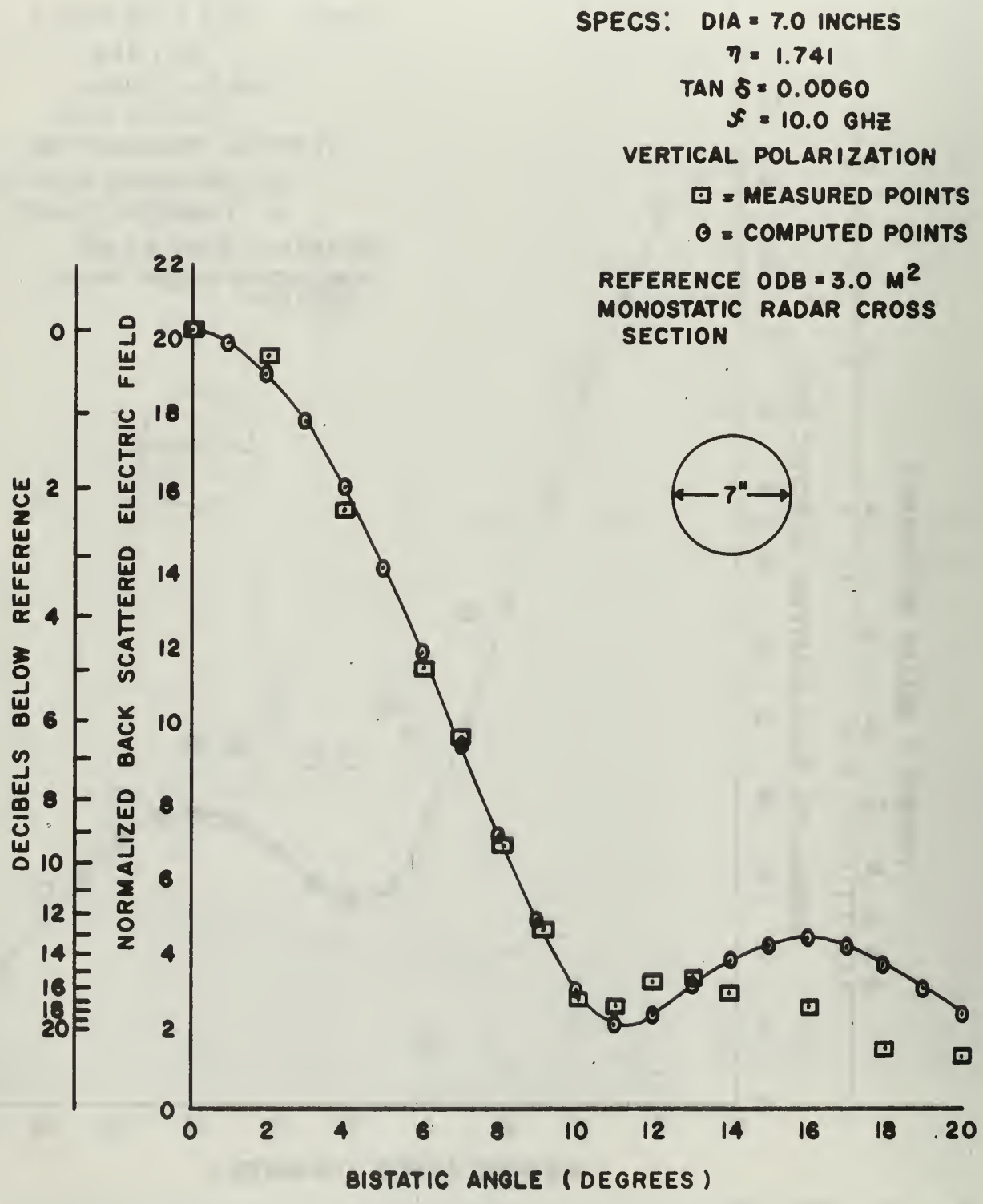
SPECS: DIA = 7.0 INCHES
η = 1.741
TAN δ = 0.0060
f = 10.0 GHZ
VERTICAL POLARIZATION
⊡ = MEASURED POINTS
θ = COMPUTED POINTS
REFERENCE ODB = 3.0 M²
MONOSTATIC RADAR CROSS SECTION
7"
DECIBELS BELOW REFERENCE
NORMALIZED BACK SCATTERED ELECTRIC FIELD
0 2 4 6 8 10 12 14 16 18 20
22 20 18 16 14 12 10 8 6 4 2 0
0 2 4 6 8 10 12 14 16 18 20
BISTATIC ANGLE (DEGREES)

Figure 6.8

RADAR CROSS SECTION vs BISTATIC ANGLE FOR A POLYSTYRENE SPHERE

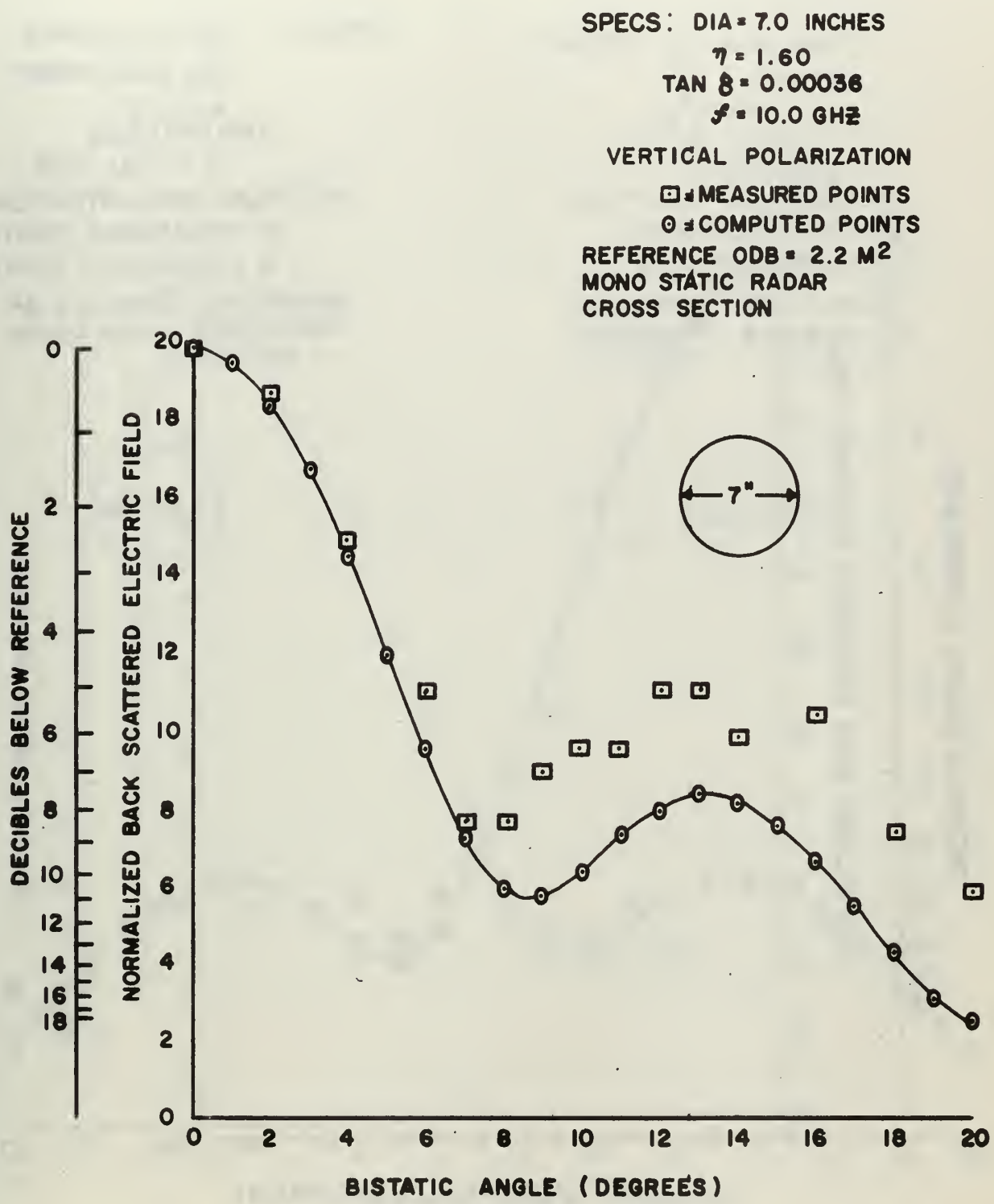

Figure 6.9

RADAR CROSS SECTION vs STATIC ANGLE FOR A LUCITE SPHEROID

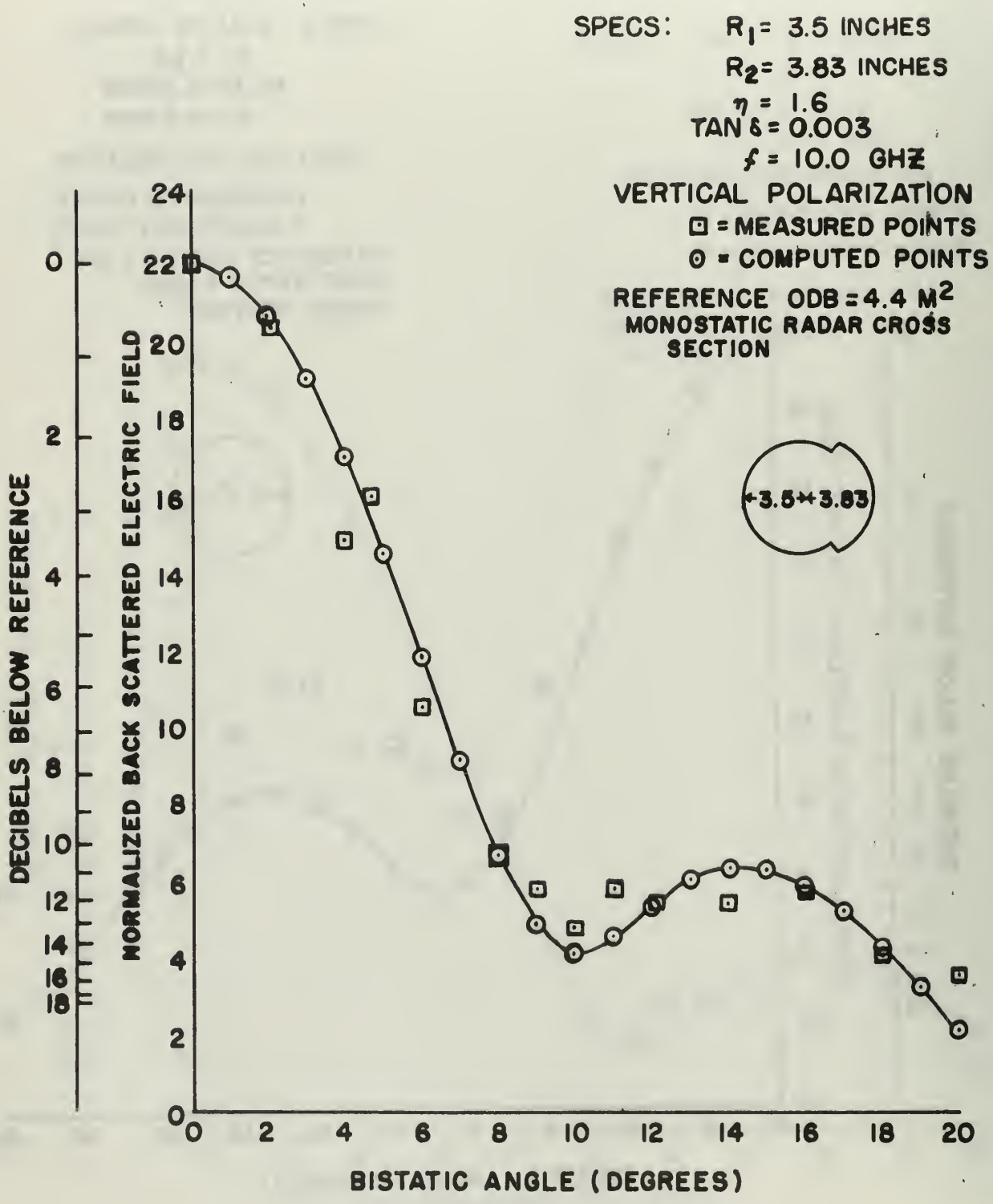

Figure 6.10

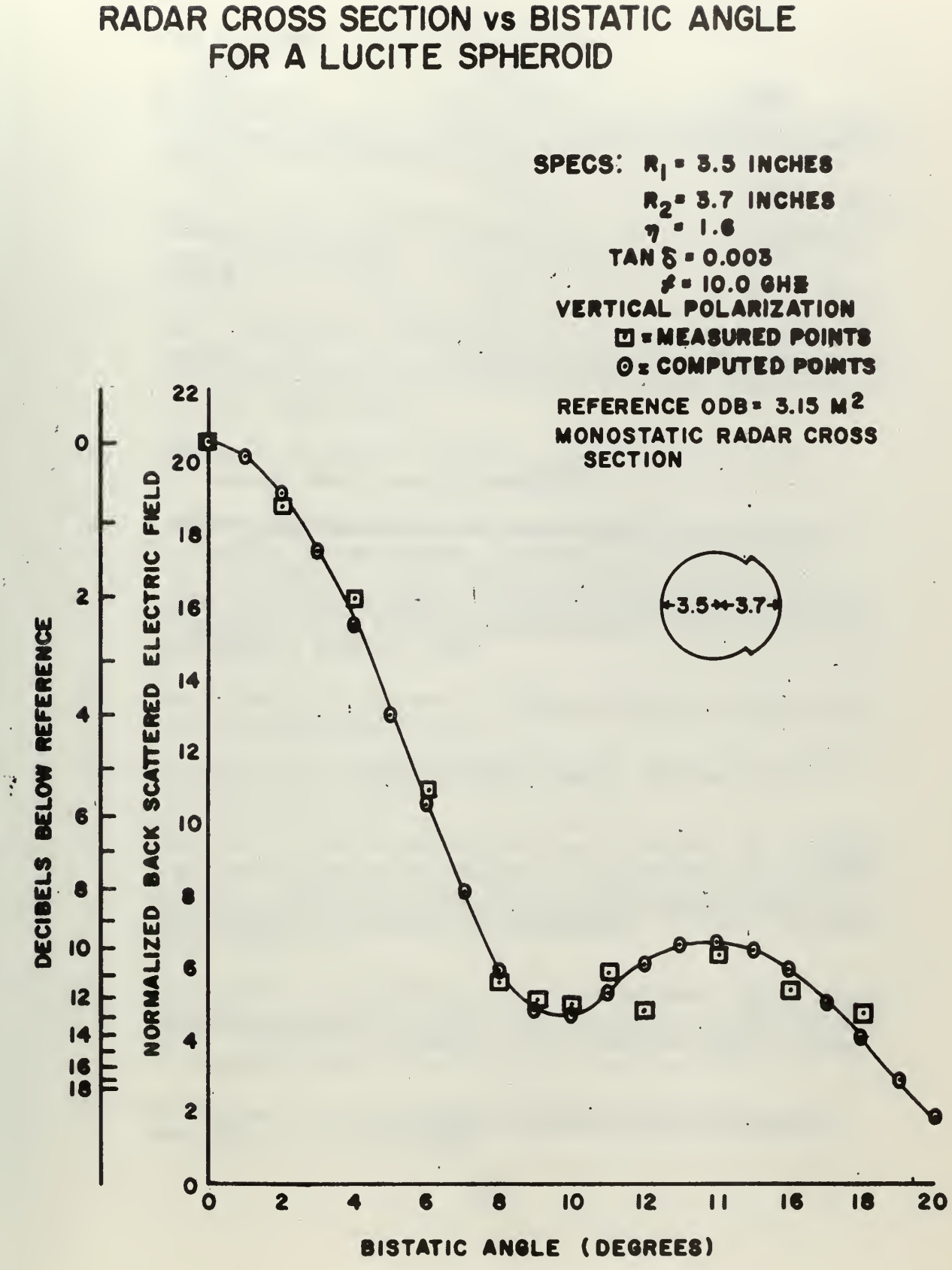
RADAR CROSS SECTION vs BISTATIC ANGLE
FOR A LUCITE SPHEROID
SPECS: R_1 = 3.5 INCHES
R_2 = 3.7 INCHES
η = 1.6
TAN δ = 0.003
f = 10.0 GHz
VERTICAL POLARIZATION
= MEASURED POINTS
= COMPUTED POINTS
REFERENCE ODB = 3.15 M^2
MONOSTATIC RADAR CROSS SECTION
3.5
3.7
DECIBELS BELOW REFERENCE
NORMALIZED BACK SCATTERED ELECTRIC FIELD
BISTATIC ANGLE (DEGREES)

Figure 6.11

Lens	Measured cross section (m^2)	Computed cross section (m^2)
Napthalene sphere	4.7	3.9
Nylon sphere	3.0	2.72
Polystyrene sphere	2.2	2.58
Lucite spheroid $R_2 = 3.7"$	3.15	2.78
Lucite spheroid $R_2 = 3.83"$	4.4	3.23

Figure 6.12

Comparison of computed and measured monostatic return

BIBLIOGRAPHY

1. Abramowitz, M. and I. Stegon. Handbook of Mathematical Functions with Formulas, Graphs and Mathematical Tables. National Bureau of Standards Applied Mathematics Series 55. 1965.

2. Atlas, D. and K. M. Glover. Backscatter by Dielectric Spheres with and without Metal Caps. Proceedings of the Interdisciplinary Conference. 1962: 213-250.

3. Atlas, D., L. J. Battan, W. G. Harper, B. M. Herman, M. Kerker, and E. Matijevic. Backscatter by Dielectric Spheres (Refractive Index, 1.6). Institute of Electrical and Electronic Engineers, Transactions on Antennas and Propogation, v. AP-11, January, 1963, Number 1.

4. Jenkins, F. A. and H. E. White. Fundamentals of Optics. McGraw-Hill Book Company, Inc., 1957.

5. Kawano, T. and L. Peters, Jr. An Extension of the Modified Geometrical Optics Methods for Radar Cross Sections of Dielectric Bodies. Report Number 1116-38. Department of Electrical Engineering: The Ohio State University Research Foundation, U. S. Department of Commerce Report AFCRL-64-714; AD 606092, 1 October, 1964.

6. Ramo S. and J. R. Whinnery. Fields and Waves in Modern Radio. John Wiley and Sons, 1953.

7. Stratton, J. A. Electromagnetic Theory. McGraw-Hill Book Company, Inc., 1941.

8. Thomas, D. T., R. G. Kouyoumjian, and L. Peters, Jr. A Modified Geometrical Optics Method for Scattering by Dielectric Bodies. Institute of Electrical and Electronic Engineers, Transactions on Antennas and Propagation, v. AP11. November, 1963. Number 6.

9. Thomas, D. T. Scattering by Dielectric Bodies. Report 11-16-20 Antenna Laboratory, Ohio State University Research Foundation. Defence Documentation Center, Defence Supply Agency. 30 October, 1962.

10. Von Hipple, A. R. Dielectric Materials and Applications. John Wiley and Sons. 1954.

APPENDIX I

DEVELOPMENT OF RAY EQUATIONS

Stationary phase

The field of an individual ray in the far zone region may be expressed in the form

(I.1) $U(\ell) = A_o \mathcal{T} F(\ell) e^{-jk\ell} e^{j\phi_o} = A_1 B_1 e^{j\phi_1}$

A_o = Reference amplitude

$\mathcal{T}$ = Total transmission coefficient

$F(\ell)$ = Spatial attenuation factor

ϕ = Phase at incidence

A_1 = Resultant amplitude

B_1 = Normalized spatial attenuation

If then, surface "S" is considered an equiphase wave front, the field at Point P may be thought of as a superposition of spherical fronts from each point on the surface of the equiphase surface by Huygen's Principle. The field at P is given by

(I.2) $U(\ell) = \frac{1}{2\lambda} \int_S U_N [1 - \cos(\hat{n}, r)] \frac{e^{-jkr}}{r} ds$

This field expression and the development of the principle of stationary phase follow that presented by Stratton. [7].

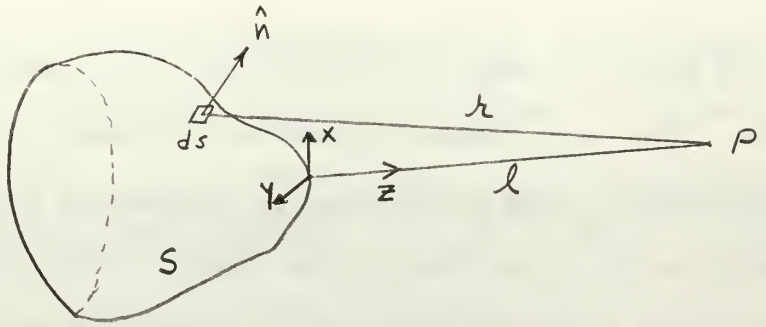

Figure I.1

Stationary phase front

Assuming that only one point exists on the surface "S", see Figure I.1, such that the normal passes through P, the field expression then becomes

$$(I.3) \quad U(\ell) = \frac{1}{2\lambda} e^{-jk} \iint_S U_N \left[1 - \cos(\hat{n}, r)\right] e^{-jk(r-\ell)} \, dx \, dy$$

The vector sum of contribution from arbitrary sections of S (λ large) will be some resultant vector as the adjacent vectors are separated by small angles. Figure I.2.a

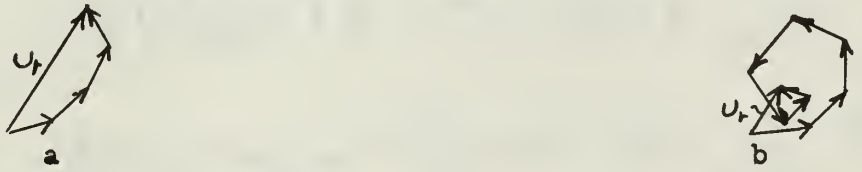

Figure I.2

Phasor addition

If the wave length is large, the vector sum will approach zero, Figure 2b. This rapid change in phase in the field results in destructive interference cancelling the contribution from an arbitrary point source on S. Phase varies slowly, however, for those portions of S in the neighborhood of N. Expressing phase as

(I.4) $\psi = (r - \ell) = [x^2 + y^2 + (\ell - z)^2]^{\frac{1}{2}} - \ell$

evaluates the attenuation F (ℓ) as

(I.5) $F(\ell) = \frac{1}{\lambda \ell} \left| \int\int_{S_N} e^{jk(r_d - \ell_s)} \right.$

The equation of the surface within S_n is

(I.6) $z = \left[\frac{x^2}{2\rho_1} + \frac{y^2}{2\rho_2} + \cdots \right]$

with ρ_1 and ρ_2 being the principle radii of curvature of the equiphase surface at the reference cross section. Substituting into Equation (I.4)

(I.7) $\psi|_{S_N} = \frac{1}{2}\left(\frac{\rho_1 + \ell}{\rho_1 \ell}\right)x^2 + \frac{1}{2}\left(\frac{\rho_2 + \ell}{\rho_2 \ell}\right)y^2$

$\psi|_{S_N}$ may be considered stationary with the vector addition taking the form of Figure 2b and $\cos(\hat{n}, r)\big|_N = 1$.

Cos $(\hat{n}, r)\big|_{N=}$ | and may be considered equal to unity within the region δ_N . The field integral thus reduces to the contribution from δ_N

(I.8) $$U(\ell) = \frac{1}{\lambda} \frac{U_N e^{-jk\ell}}{\ell} \int\int_{\delta_N} e^{-jk(r-\ell)} \, d\delta$$

Therefore

(I.9) $$F(\ell) = \int\int_{\delta_N} e^{-jk\psi} \, d\delta$$

If ψ has but one stationary point on the surface, the field at P becomes

(I.10) $$U(\ell) = \frac{1}{\lambda\ell} U_N e^{-jk\ell} \int\int_{-\infty}^{\infty} e^{-\frac{jk}{2}\left[\left(\frac{\rho_1+\ell}{\rho_1\ell}\right)x^2 + \left(\frac{\rho_2+\ell}{\rho_2\ell}\right)y^2\right]} dx\,dy$$

Transformation to Fresnel integrals:

(I.11) $$\int_{-\infty}^{\infty} e^{-j\frac{\pi}{2}\xi^2} d\xi = \sqrt{2}\, e^{-j\frac{\pi}{4}}$$

gives

(I.12) $$U(\ell) = \frac{1}{\lambda\ell} U_N e^{-jk\ell} \int e^{-\frac{jk\ell}{2}\left(\frac{\rho_1+\ell}{\rho_1\ell}\right)x^2} \int e^{-j\frac{k\ell}{2}\left(\frac{\rho_2+\ell}{\rho_2\ell}\right)y^2} dy$$

(I.13) $$F(\ell) = \frac{1}{2\lambda\ell}\left[\frac{\rho_1\rho_2}{(\rho_1+\ell)(\rho_2+\ell)}\right]^{\frac{1}{2}}$$

and

(I.14) $$B_1 = \frac{1}{\lambda}\left[\frac{\rho_1\rho_2}{(\rho_1+\ell)(\rho_2+\ell)}\right]^{\frac{1}{2}}$$

which is identical to the form obtained for geometric optics. For those wave fronts with two radii of curvature, geometric optics apply and the form

(I.15) $$B = \frac{1}{\lambda}\left[\frac{\rho_1\rho_2}{(\rho_1+\ell)(\rho_2+\ell}\right]^{\frac{1}{2}}$$

is used. Non Gaussian wave fronts, however, such as the ring sources for the stationary and glory rays require evaluation of the integral form.

(I.16) $$F(\ell) = \frac{1}{2\lambda\ell}\iint_{SW} e^{-jk\psi}dS$$

Rear axial ray

The spatial attenuation for the rear axial ray $F(\ell)_3$ is derived as follows: (See Figure I.3)

(I.17) $$\mathcal{B} = \left[-2(q+1)\theta_1 + 2\theta_0 + \pi q\right]$$ q = number of internal reflection

(I.18) $$\frac{d\beta}{d\theta_0} = -2(q+1)\frac{d\theta_1}{d\theta_0} + 2 = 0$$

$$\frac{d\theta_0}{d\theta_1} = q + 1$$

$$\sqrt{\epsilon_{r_1}}\sin\theta_1 = \sqrt{\epsilon_{r_0}}\sin\theta_0 = \sin\theta_0$$

(I.19) $$\frac{d\theta_0}{d\theta_1} = \frac{\sqrt{\epsilon_{r_1}}\cos\theta_1}{\sqrt{1-\epsilon_{r_1}\sin^2\theta_0}} = \frac{\sqrt{\epsilon_{r_1}}\cos\theta_1}{\cos\theta_0} \equiv p$$

therefore

(I.20) $$p = q + 1$$

(I.21) $$F(l) = \sqrt{\frac{\rho_1\rho_2}{(U_1)(l)}}\sqrt{\frac{a\sin\theta_0}{l\sin\beta}}$$

(I.22) $$\rho_1 = \frac{a\,p\cos\theta_1}{p-1}$$

(I.23) $$U_1 = \frac{a(2-p)\cos\theta_1}{p-1}$$

(I.24) $$\rho_2 = \frac{(a\cos\theta_0)(4-p)}{2(p-2)}$$

(I.25) $$F(l)_3 = \sqrt{\frac{p\sin 2\theta_0}{(2-p)\sin\beta}}\,\frac{a}{2l}$$

(I.26) $$\lim_{\beta \to 180^\circ} \sqrt{\frac{\sin 2\theta_0}{\sin \beta}} = \sqrt{\frac{\rho}{2-\rho}}$$

(I.27) $$F(l)_3 = \frac{\partial}{2l}\left(\sqrt{\frac{\rho}{2-\rho}}\right)^2 = \frac{\partial}{2l}\,\frac{\sqrt{\epsilon_\lambda}}{2-\sqrt{\epsilon_\lambda}}$$

(I.28) $$B = \frac{\sqrt{\epsilon_\lambda}}{2-\sqrt{\epsilon_\lambda}} = \frac{\nu}{2-\nu}$$

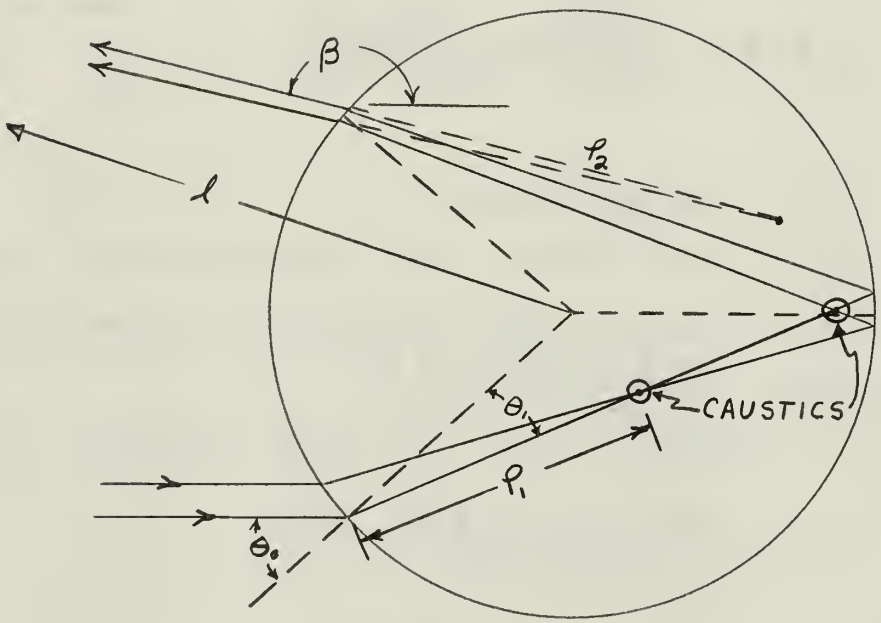

Figure I.3

Rear axial ray

Stationary ray

The stationary rays may be expressed as a cubic wave front as shown in Figure I.4. The equation of the wave front is $\frac{hv^3}{3a^2}$ where a is the sphere radius, h is a constant and v the distance along the target as shown. This development and notation is presented by Thomas. [9].

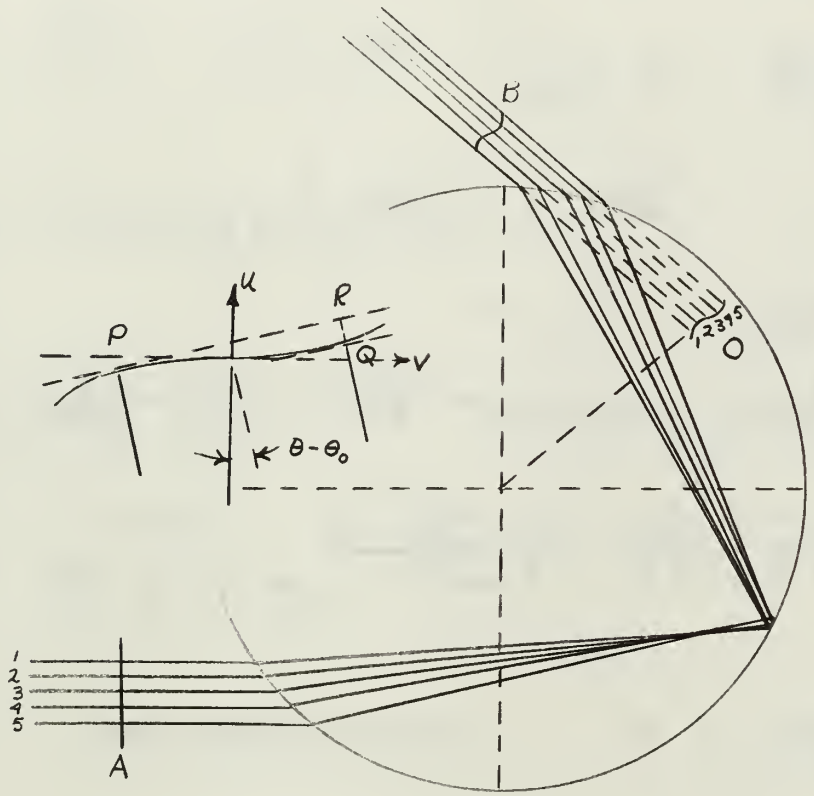

Figure I.4

Stationary ray

The emergent angle for the single internally reflected ray is

(I.29) $\Theta = 3r' - r$

The stationary ray occurs when Θ is a minimum, i.e.

(I.30) $\frac{d\Theta}{dr} = 0$

$$\frac{d\Theta}{dr} = 3\frac{dr'}{dr} - 1$$

(I.31) $$\frac{d^2\Theta}{dr} = 3\frac{d^2r'}{dr^2}$$

$$\sin r = \sqrt{\epsilon_r}\sin r' \frac{dr'}{dr}$$

(I.32) $$\frac{d\sin r}{dr} = \cos r$$

$$\frac{d\sin r}{dr} = \sqrt{\epsilon_r}\left[\cos r'\left(\frac{dr'}{dr}\right)^2 + \sin r \frac{d^2r'}{dr^2}\right]$$

(I.33) $$\frac{d^2r}{dr} = \frac{dr'}{dr}\,\frac{\left[1 - \left(\frac{dr'}{dr}\right)^2\right]}{\tan r}$$

(I.34) $$\left.\frac{d\Theta}{dr}\right|_{r=r_0} = 0$$ for the stationary ray

(I.35) $\Theta = 3r' - r$

$$\frac{d\Theta}{dr} = 3\frac{dr'}{dr} - 1$$

(I.36) $$\left.\frac{dr'}{dr}\right|_{r=r_0} = \frac{1}{3}$$

(I.37) $$\left.\frac{d^2r}{dr}\right|_{r=r_0} = \frac{1}{3}\left[\frac{1-\left(\frac{1}{3}\right)^2}{\tan r_0}\right]$$

$$\left.\frac{d^2r}{dr^2}\right|_{r=r_0} = \frac{8}{27\tan r_0}$$

(I.38) $$\frac{d^2\theta}{dr^2} = \frac{8}{9\tan r_0}$$

(I.39) $$\theta-\theta_0 \approx \frac{8}{9\tan r_0}(r-r_0)^2$$

(I.40) $$U \equiv \frac{hv^3}{3a^2}$$ cubic wave front

for small v

(I.41) $$\frac{dU}{dV} = \theta-\theta_0$$

(I.42) $$V = a\cos r - a\cos r_0$$

$$v \approx -a(r-r_0)\sin r_0$$

(I.43) $$\frac{dU}{dV} = \frac{8V^2}{9a^2\sin^2 r_0 \tan r_0}$$

(I.44) $$U = \frac{8V^3}{27\partial^2 \sin^2 r_0 \tan r_0}$$

(I.45) $$h = \frac{8}{9 \sin^2 r_0 \tan r_0}$$

(I.46) $$\psi = V(\theta - \theta_0) + \frac{hV^3}{3\partial^2}$$

θ of interest $= \pi$

$u = r - r_0$

(I.47) $$F(l) = \frac{2\pi r_0}{\lambda l} \int_{-\infty}^{\infty} (r - r_0)(\theta - \theta_0) - \frac{h(r - r_0)^3}{3\partial^2} dr$$

$$s \equiv \left(\frac{\partial^2}{k_0 h}\right)^{1/3} \qquad t \equiv \frac{r - r_0}{s} \qquad z \equiv k_0 s (\theta - \theta_0)$$

(I.48) $$F(l) = \frac{s}{\lambda l} \left| \int_{-\infty}^{\infty} e^{-t\left(zt - \frac{t^3}{3}\right)} dt \right| 2\pi r_0$$

(I.49) $$A_i(z) = \frac{1}{2} \int_{-\infty}^{\infty} e^{-i\left(zt - \frac{t^3}{3}\right)} dt$$ Airy function. Tabulated [1]

(I.50) $$F(l) = \frac{4\pi r_0}{\lambda l} s \left| Ai(z) \right|$$

APPENDIX II

SAMPLE COMPUTER PROGRAM

```
      PROGRAM BACKSCATTER
      DIMENSION R(100),TAUH(100),TAUV(100),PHI(100),X0(100),RHO1(100),
     1XLM(100),CPHI(100),SPHI(100),XLA(100)
      DIMENSION RHO2(100),X11(100),ZETA(100),SZETA(100),CZETA(100)
      DIMENSION REFV(100),REFH(100)
      DIMENSION TRAH12(100),TRAV12(100),TRAH21(100),TRAV21(100)
      DIMENSION FAC(100)
      PRINT 1111
 1111 FORMAT(1H1///17X,3HPHI,16X,4HTAUH,16X, 4HTAUV,16X,4HRHO1//)
      PI=3.14159
      R1=3.5
      ZN=1.6
      B=3.5
      R2=3.5
      TDEL=0.00036
      N=1
      XN=N
      DO 100 I=1,N
      XI=I
      R(I)=R1*SQRTF(XI/XN)
      IF(I-1) 50,40,50
   40 Y1 =R(1)/2.
      GO TO 60
   50 Y1 = (R(I-1) +R(I))/2.
   60 X1 =R1-SQRTF(R1**2-Y1**2)
      X11(I)=X1
      RHO2(I)=Y1
      XLAMDA=-ATANF(Y1/(X1-R1))
      ZETA(I)=XLAMDA*2.
      SZETA(I)=SINF(ZETA(I))
      CZETA(I)=COSF(ZETA(I))
      XLAMPR=ASINF(SINF(XLAMDA)/ZN)
      REFV(I)=TANF(XLAMDA-XLAMPR)/TANF(XLAMDA+XLAMPR)
      REFH(I)=-SINF(XLAMDA-XLAMPR)/SINF(XLAMDA+XLAMPR)
      TRAH12(I)=2.*SINF(XLAMPR)*COSF(XLAMDA)/SINF(XLAMDA+XLAMPR)
      TRAV12(I)=TRAH12(I)/COSF(XLAMDA-XLAMPR)
      TRAH21(I)=2.*SINF(XLAMDA)*COSF(XLAMPR)/SINF(XLAMDA+XLAMPR)
      TRAV21(I)=TRAH21(I)/COSF(XLAMPR-XLAMDA)
      TAUH(I)=TRAH12(I)*TRAH21(I)
```

```
      TAUV(I)=TRAV12(I)*TRAV21(I)
      XK1=TANF(ATANF(-Y1/(R1-X1))+XLAMPR)
      AA=1.+XK1**2
      BB=-2.*(B+XK1**2*X1-Y1*XK1)
      GAMMA=B**2-R2**2+XK1**2*X1**2-2.*Y1*XK1*X1+Y1**2
      X2=(-BB+SQRTF(BB**2-4.*AA*GAMMA))/(2.* AA)
      Y2=XK1*(X2-X1)+Y1
      XM2=(R-X2)/Y2
      XK2=TANF(2.*ATANF(XM2)-ATANF(XK1))
      A1=1.+XK2**2
      B1=-2.*(R1+XK2**2*X2-Y2*XK2)
      GAMMA1=XK2**2*X2**2-2.*Y2*XK2*X2+Y2**2
      X0(I)=(-B1-SQRTF(B1**2-4.*A1*GAMMA1))/(2.*A1)
      RHO0=XK2*(X0(I)-X2)+Y2
      XM3=(R1-X0(I))/RHO0
      PHI(I)=      ATANF(XM3)-XLAMDA+PI/2.
      PHI1=ABSF(PHI(I))
      SPHI(I)=SINF(PHI1)
      CPHI(I)=COSF(PHI1)
      RHO1(I)=ABSF(RHO0)
      XLA(I)=X1+1.
      XLM(I)=2.*ZN*SQRTF((X2-X1)**2+(Y1-Y2)**2)
      FAC(I)=EXPF(-PI*TDEL*XLM(I)*2.54/3.0)
      PHIDEG=PHI(I)*180./PI
      PRINT 1000,PHIDEG,TAUH(I),TAUV(I),RHO1(I)
 1000 FORMAT(4F20.6)
  100 CONTINUE
      PRINT 2000
 2000 FORMAT (1H1///17X,3HPSI,18X,2HEF,14X,6HTHETAF,16X,2HDB//)
      DO 500 J=1,21
      XJ=J
      PSI=(-1.+XJ)*PI/180.
      CPSI=COSF(PSI)
      SPSI=SINF(PSI)
      EXSUM=0.
      EYSUM=0.
      DO 400 I=1,N
      IF (PHI(I)) 250,270,270
  250 CON=PI
      GO TO 280
  270 CON=0.
  280 DO 300 K=1,36
      XK=K
      THETA=(-92.5+5.*XK)*PI/180.
      CTHETA=COSF(THETA)
```

```
      STHETA=SINF(THETA)
      CTHESQ=CTHETA**2
      STHESQ=STHETA**2
      CGAM=SPSI*SPHI(I)*SINF(THETA+CON)+CPSI*CPHI(I)
      CBET=SPSI*SZETA(I)*STHETA+CPSI*CZETA(I)
      IF(CZETA(I)) 285,285,290
  285 ER=0.
      GO TO 295
  290 CONTINUE
      ER=REFV(I)*CTHESQ+REFH(I)*STHESQ
  295 CONTINUE
      ERT=ER*CBET**2
      ET=TAUV(I)*CTHESQ+TAUH(I)*STHESQ
      E=ET*FAC(I)*CGAM**2
      D=ABSF(RHO1(I)*STHETA*SPSI+CPSI*(-X0(I)-1.))
      PHASE=(120.*2.54*(XLA(I)+XLM(I)+D))
      PHAS=PHASE*PI/180.
      DR=ABSF(RHO2(I)*STHETA*SPSI+CPSI*(-X11(I)-1.))
      PHASR=(120.*2.54*(XLA(I)+DR) )
      PHAR=PHASR*PI/180.
      EX=E*COSF(PHAS)+ERT*COSF(PHAR)
      EY=E*SINF(PHAS)+ERT*SINF(PHAR)
      EXSUM=EXSUM+EX
      EYSUM=EYSUM+EY
  300 CONTINUE
  400 CONTINUE
      EF=SQRTF(EYSUM**2+EXSUM**2)
      IF(J-1)420,410,420
  410 EF1=EF
  420 DB=8.68388*LOGF(EF/EF1)
      THETAF=ATANF(EXSUM/EYSUM)*180./PI
      PSI=PSI*180./PI
      PRINT 3000,PSI,EF,THETAF,DB
 3000 FORMAT(4F20.6)
  500 CONTINUE
      END
```

INITIAL DISTRIBUTION LIST

		No. Copies
1.	Defense Documentation Center Cameron Station Alexandria, Virginia 22134	20
2.	Library U. S. Naval Postgraduate School Monterey, California	2
3.	Chief of Naval Operations (OP-94) Department of the Navy Washington, D. C. 20350	1
4.	Professor Paul E. Cooper Department of Electrical Engineering U. S. Naval Postgraduate School Monterey, California	1
5.	Micronetics, Inc. 7155 Mission Gorge Road San Diego, California	1
6.	Mr. Keith Rosendahl Avionics Division U. S. Naval Missile Test Center Point Mugu, California	1
7.	Lcdr. Herbert Segelhorst 248 Beach Road Marina, California 93933	1
8.	Cdr. John Ambrose 3034 Stevenson Drive Pebble Beach, California 93953	1

Unclassified
Security Classification

DOCUMENT CONTROL DATA - R&D

(Security classification of title, body of abstract and indexing annotation must be entered when the overall report is classified)

1. ORIGINATING ACTIVITY *(Corporate author)*
U. S. Naval Postgraduate School
Monterey, California 93940

2a. REPORT SECURITY CLASSIFICATION
Unclassified

2b. GROUP
N.A.

3. REPORT TITLE
Microwave Backscatter from a Capped Dielectric Lens

4. DESCRIPTIVE NOTES *(Type of report and inclusive dates)*
Thesis for Masters Degree in Communications Engineering, May 1966

5. AUTHOR(S) *(Last name, first name, initial)*
Ambrose, John E. Commander U. S. Navy
Segelhorst, Herbert E. Lieutenant Commander U. S. Navy

6. REPORT DATE	7a. TOTAL NO. OF PAGES	7b. NO. OF REFS
May 1966	90	10

8a. CONTRACT OR GRANT NO.

b. PROJECT NO.

c.

d.

9a. ORIGINATOR'S REPORT NUMBER(S)

9b. OTHER REPORT NO(S) *(Any other numbers that may be assigned this report)*

10. AVAILABILITY/LIMITATION NOTICES
All distribution of this report is controlled. Qualified DDC users shall request through: Superintendent, U. S. Naval Postgraduate School, Monterey, California 93940

This document has been approved for public release and sale; its distribution is unlimited. *

11. SUPPLEMENTARY NOTES
[redacted]

12. SPONSORING MILITARY ACTIVITY
U. S. Naval Postgraduate School
Monterey, California 93940

13. ABSTRACT

A specific application of a spherical dielectric lens provides the impetus for the development of a simple analytical method of predicting microwave backscatter from such a lens. The principles of geometric optics and stationary phase are presented as detailed in current literature. Geometric optics or ray tracing is then utilized in developing a unique method of determining the backscattered E field by the use of a computer program constructed for the CDC 1604 computer. Several models are constructed and tested in an anechoic chamber and on an outdoor radar backscatter range. The results of these tests are then compared to those of the computer program. The correlation of the predicted and measured E fields indicate the computer program to be a useful tool in the construction of a dielectric lens.

[redacted]

Released by Micronetics as of 1/1/70 GRL

DD FORM 1 JAN 64 1473

Unclassified
Security Classification

14. KEY WORDS	LINK A		LINK B		LINK C	
	ROLE	WT	ROLE	WT	ROLE	WT
Dielectric lens						
Radar augmentation						
Radar backscatter						
Bistatic angle						

INSTRUCTIONS

1. ORIGINATING ACTIVITY: Enter the name and address of the contractor, subcontractor, grantee, Department of Defense activity or other organization *(corporate author)* issuing the report.

2a. REPORT SECURITY CLASSIFICATION: Enter the overall security classification of the report. Indicate whether "Restricted Data" is included. Marking is to be in accordance with appropriate security regulations.

2b. GROUP: Automatic downgrading is specified in DoD Directive 5200.10 and Armed Forces Industrial Manual. Enter the group number. Also, when applicable, show that optional markings have been used for Group 3 and Group 4 as authorized.

3. REPORT TITLE: Enter the complete report title in all capital letters. Titles in all cases should be unclassified. If a meaningful title cannot be selected without classification, show title classification in all capitals in parenthesis immediately following the title.

4. DESCRIPTIVE NOTES: If appropriate, enter the type of report, e.g., interim, progress, summary, annual, or final. Give the inclusive dates when a specific reporting period is covered.

5. AUTHOR(S): Enter the name(s) of author(s) as shown on or in the report. Enter last name, first name, middle initial. If military, show rank and branch of service. The name of the principal author is an absolute minimum requirement.

6. REPORT DATE: Enter the date of the report as day, month, year; or month, year. If more than one date appears on the report, use date of publication.

7a. TOTAL NUMBER OF PAGES: The total page count should follow normal pagination procedures, i.e., enter the number of pages containing information.

7b. NUMBER OF REFERENCES: Enter the total number of references cited in the report.

8a. CONTRACT OR GRANT NUMBER: If appropriate, enter the applicable number of the contract or grant under which the report was written.

8b, 8c, & 8d. PROJECT NUMBER: Enter the appropriate military department identification, such as project number, subproject number, system numbers, task number, etc.

9a. ORIGINATOR'S REPORT NUMBER(S): Enter the official report number by which the document will be identified and controlled by the originating activity. This number must be unique to this report.

9b. OTHER REPORT NUMBER(S): If the report has been assigned any other report numbers *(either by the originator or by the sponsor)*, also enter this number(s).

10. AVAILABILITY/LIMITATION NOTICES: Enter any limitations on further dissemination of the report, other than those imposed by security classification, using standard statements such as:

(1) "Qualified requesters may obtain copies of this report from DDC."

(2) "Foreign announcement and dissemination of this report by DDC is not authorized."

(3) "U. S. Government agencies may obtain copies of this report directly from DDC. Other qualified DDC users shall request through _____."

(4) "U. S. military agencies may obtain copies of this report directly from DDC. Other qualified users shall request through _____."

(5) "All distribution of this report is controlled. Qualified DDC users shall request through _____."

If the report has been furnished to the Office of Technical Services, Department of Commerce, for sale to the public, indicate this fact and enter the price, if known.

11. SUPPLEMENTARY NOTES: Use for additional explanatory notes.

12. SPONSORING MILITARY ACTIVITY: Enter the name of the departmental project office or laboratory sponsoring *(paying for)* the research and development. Include address.

13. ABSTRACT: Enter an abstract giving a brief and factual summary of the document indicative of the report, even though it may also appear elsewhere in the body of the technical report. If additional space is required, a continuation sheet shall be attached.

It is highly desirable that the abstract of classified reports be unclassified. Each paragraph of the abstract shall end with an indication of the military security classification of the information in the paragraph, represented as *(TS)*, *(S)*, *(C)*, or *(U)*.

There is no limitation on the length of the abstract. However, the suggested length is from 150 to 225 words.

14. KEY WORDS: Key words are technically meaningful terms or short phrases that characterize a report and may be used as index entries for cataloging the report. Key words must be selected so that no security classification is required. Identifiers, such as equipment model designation, trade name, military project code name, geographic location, may be used as key words but will be followed by an indication of technical context. The assignment of links, roles, and weights is optional.

DD FORM 1 JAN 64 1473 (BACK)

NOT FOR LOAN

thesA4295
Microwave backscatter from a capped diel
3 2768 001 89860 4
DUDLEY KNOX LIBRARY